Biological and chemical signs of upward motions in permanent geostrophic fronts of the western Mediterranean

Bruno Zakardjian, Louis Prieur

JOURNAL OF GEOPHYSICAL RESEARCH, VOL. 103, NO. C12, PAGES 27,849–27,866, NOVEMBER 15, 1998

Biological and chemical signs of upward motions in permanent geostrophic fronts of the Western Mediterranean

Bruno Zakardjian

Institut National de la Recherche Scientifique, Océanologie, Université du Québec à Rimouski, Québec, Canada

Louis Prieur

Laboratoire de Physique et Chimie Marines, Observatoire Océanologique, CNRS, Universite Paris VI Villefranche-sur-Mer, France

Abstract. Upward motions are often invoked to explain the high productivity of permanent geostrophic fronts in the Western Mediterranean while physical evidence of such upward advections is seldom reported. The goal of this study is to define biological and chemical criteria, which can be used to localize such upward motions zones. We use a one-dimensional, time-dependent model of phytoplankton dynamics to test the effects of upward advection on the vertical distribution of phytoplankton biomass, nutrients, and dissolved oxygen. Simulations also include the effects of advective motions of the phytoplankton cells in the light field on phytoplankton growth. In conformance with the continuity equation, boundary conditions were defined to allow horizontal flow of the upwelled water within the upper mixed layer. Low upward advections (≤ 3 m d^{-1}) led to a shallowing and sharpening of the nitracline, oxycline, and deep maxima of phytoplankton biomass and oxygen and to an increase in phytoplankton biomass. By confining the phytoplankton-nutrient system in the surface mixed layer, higher upward advections lead to homogeneous phytoplankton biomass and oxygen vertical distributions in the upper mixed layer, the nitracline and the oxycline being then at the top of the pycnocline. Data collected during the Prolig 2 cruise (May 1985) on the heavy side of the Liguro-Provençal front are interpreted as an illustration of these numerical results. Computed primary production rates are compared with measurements conducted in the Almería-Oran front during the Almofront 1 cruise (April 1991) in a similar situation. In both fronts, upward advections of 1–2 m d^{-1} would be sufficient to account for the observed vertical distributions and the increased primary production. Ecological implications for the phytoplankton-nutrient system are discussed, particularly the spatial uncoupling of phytoplankton biomass and primary production in permanent geostrophic fronts.

1. Introduction

The Liguro-Provençal front [*Béthoux et Prieur*, 1983; *Sournia et al.*, 1990] and the Almería-Oran front [*Cheney and Doblar*, 1982; *Tintoré et al.*, 1988] are permanent geostrophic structures in the Western Mediterranean. Both fronts are areas of high-plankton biomass, in contrast with two adjacent oligotrophic-type systems [*Lohrenz et al.*, 1988; *Tintoré et al.*, 1988; *Sournia et al.*, 1990; *Prieur et al.*, 1993; *Claustre et al.*, 1994b], and show net change in both the specific composition of the autotrophic [*Claustre et al.*, 1994b] and the heterotrophic [*Boucher et al.*, 1987; *Thibault et al.*, 1994] communities. Several features indicate that the two fronts are sites of enhanced production in response to geostrophic frontal dynamics. In addition to the main geostrophic flow, a secondary circulation exists, i.e., the ageostrophic flow, which is characterized by enhanced vertical advections as shown for example by *Dewey et al.* [1991] in the California Current. It is thought that upward advections in the frontal zone upwell nutrients into the photic zone and enhance primary production [*Lohrenz et al.*, 1988; *Videau et al.*, 1994]. The resulting high biomass is then downwelled by the convergent part of the ageostrophic circulation along the isopycnals [*Claustre et al.*, 1994a, b; *Videau et al.*, 1994]. However, physical evidence for upward advection in the two fronts is not well-documented (see, however, *Tintoré et al.* [1991] and *Viudez and Tintoré* [1996]) and poorly understood. This paper defines criteria from the vertical distribution of parameters involved in primary production, which can be used to localize, with some confidence, the upward motions in such frontal zones.

In a previous modeling study [*Zakardjian and Prieur*, 1994], two types of phytoplankton-nutrient systems resulting from high- and low-turbulent regimes (HTR and LTR, respectively) were described, with the LTR representing the ecological conditions in the waters adjacent to the Liguro-Provençal and Almería-Oran fronts, where the vertical structure is controlled by diffuse vertical fluxes. We use a modified version of this previous one-dimensional vertical model (presented in section 2) to test the sensitivity of the LTR system when an upward advection term is added. In section 3 we describe the steady state vertical distribution of phytoplankton biomass, nutrients, and dissolved oxygen obtained with upward advection values ranging from 0 to 5 m d^{-1}. Effects of upward advection on the vertical distribution of primary production, on phytoplankton growth, and, finally, on the productivity indexes of the water column are detailed. In section 4 we present multiparametric

Paper number 98JC01537.
0148-0227/98/98JC-01537$09.00

data collected on the Liguro-Provençal front during the Prolig 2 cruise (May–June 1985) to illustrate the numerical results, and we compare the simulated enrichment by upward advection with primary production measurements conducted during the Almofront 1 cruise (April–May 1991) in the Almería-Oran front. Biological and chemical criteria for upward advection are defined and discussed section 5. These results indicate a possible spatial uncoupling of phytoplankton biomass and primary production at small scales as the consequence of the upwelled component of the secondary circulation.

2. Formulation of the Model

2.1. Basis

Assuming stationary physical conditions, light, stratification, vertical turbulent mixing and upward advection, the vertical distribution of phytoplankton biomass (B), nitrate (NO_3), nitrite (NO_2), ammonia (NH_4), and dissolved oxygen (O_2) concentrations are computed from the set of differential equations given in the appendix. Physical processes, phytoplankton growth rate (μ), and nutrient assimilation by phytoplankton (S_{NH4}, S_{NO3}, and S_{NO2}) are detailed in the following sections. Other processes already described by *Zakardjian and Prieur* [1994] are briefly presented here (see appendix and Table 1 for formulations and parameters). The grazing pressure (Graz) is defined with a modified Ivlev-type function (equation (A8)) [*Franks et al.*, 1986b] and a depth- and time-constant biomass of herbivorous zooplankton. To take into account the regeneration of nitrogen in the photic layer, a constant fraction (0.6) of the grazed phytoplankton nitrogen is regenerated in terms of ammonia (equation A4). Following the reasoning of *Pomeroy and Wiebe* [1988], this constant fraction was defined assuming a two-step food web (for example, ciliates grazing on phytoplankton and copepods grazing on ciliates and phytoplankton) with a growth efficiency of 70% for each step [e.g., *Frost*, 1980; *Berggreen et al.*, 1988; *Kiørboe*, 1989]. The remaining fraction of grazed and nonregenerated nitrogen is computed as a biologically exported matter (BEM) in (A7). The fate of this biological matter obeys to processes affecting the upper food steps (predator-prey interactions, sedimentation and regeneration of detrital matter, etc.) that have no or little effects on the local primary production at a short time scale. The fate of this biologically exported matter is not considered in the model. The model includes ammonia and nitrite oxidation via nitrification processes (equations A9 and A10) following the formulations of *Olson* [1981]. In addition, the model distinguishes between new and regenerated production, where phytoplankton production is sustained by NO_3 and NH_4-NO_2, respectively. Using standard stochiometric ratios, the concentration of dissolved oxygen depends on these biochemical processes (equation A5), and is also subjected to ocean-atmosphere exchange at the upper boundary layer (equation A11). Nutrients and phytoplankton biomass are computed in mmol N m^{-3}, and dissolved oxygen concentrations are computed in mmol O_2 m^{-3}. Primary production terms and dissolved oxygen concentrations are converted to mg C m^{-3} d^{-1} and mL L^{-1}, respectively, to facilitate comparisons with observed data. Conversion to units of carbon is made with the molar ratio C/N = 106/16 [*Redfield et al.*, 1963].

2.2. Physical Processes

The model is a diagnostic tool which assumes a stationary vertical stratification and is used to evaluate the influence of upward fluxes of nutrients through isopycnals. This stationary hypothesis comes from several coupled, ecological-physical observations made on permanent geostrophic fronts of the Western Mediterranean as discussed in section 5. This hypothesis can be interpreted in two ways: (1) The imposed upward advection corresponds to a conceptual diapycnal flux, or (2) the upward advection of isopycnals is balanced by a negative buoyancy flux. In general, the hypothesis would be valid as much as the stratification changes remain ecologically insignificant.

The vertical diffusion coefficient ($K(z)$) is estimated from a stationary density field using the following classical formulations [*Osborn*, 1980]:

$$K(z) = \frac{0.25\varepsilon(z)}{N(z)^2} \tag{1}$$

$$N^2(z) = -\frac{g}{\rho_w}\frac{\partial \rho}{\partial z} \tag{2}$$

$$z = \begin{cases} 20\text{–}200 \text{ m} & \varepsilon(z) = a_0 N(z) \\ 0\text{–}19 \text{ m} & \varepsilon(z) = \varepsilon(20) \end{cases} \tag{3}$$

where $\varepsilon(z)$ is the turbulent kinetic energy (TKE) dissipation rate, $N(z)$ is the buoyancy frequency, g is the acceleration due to gravity (g = 9.82 m s^{-2}), ρ_w is a reference water density (1029 kg m^{-3} for the Western Mediterranean) and $\partial\rho/\partial z$ is the vertical density gradient. The density gradient used in (2) was defined with analytical functions [e.g., *Zakardjian and Prieur*, 1994] whose parameters were adjusted to fit density profiles observed at selected stations on the heavy side of the Liguro-Provençal front (Figure 1a). The main pycnocline of the profile used in the model was fitted to observations, and we imposed an upper well-mixed layer (10 m depth), which was not found on the observed profiles, for reasons exposed later in this section.

The TKE dissipation rate, which links the turbulent regime and stratification of the water column through (1), depended linearly on $N(z)$ from the pycnocline to the bottom and was assumed constant above the main pycnocline ((3), see Figure 1b). This leads to a diffusivity $K(z)$, which is inversely related to $N(z)$ below the pycnocline and implies turbulent diffusion due to internal waves breaking [e.g., *Gargett and Holloway*, 1984]. Above the pycnocline, the source of energy for turbulent mixing in the imposed well-mixed layer is more likely to be a function of the surface wind stress. The a_0 parameter value was fixed to have a TKE dissipation rate of 10^{-8} m^2 s^{-3} at depth (Figure 1b). With this depth variation of ε, the turbulent diffusion coefficient $K(z)$ (Figure 1c) reached a maximum value of 2000 m^2 d^{-1} (2.31 10^2 cm^2 s^{-1}) in the upper well-mixed layer [e.g., *Denman and Gargett*, 1983; *Lande and Wood*, 1987] and strongly decreased in the main pycnocline to a minimum value of 5 m^2 d^{-1} (0.58 cm^2 s^{-1}). Below the main pycnocline, $K(z)$ slightly increased, because of the decreased stratification, and reached a maximum value of 45 m^2 d^{-1} (5.2 cm^2 s^{-1}) at depth. Increasing $K(z)$ below the subsurface pycnocline is inherent in the parameterization and would be due to decreasing buoyancy [e.g., *Moum and Osborn*, 1986]. The use of such eddy diffusivity parameterization is still under discussion (see *Gaspar et al.* [1988] or *Cummins et al.* [1990]), but similar vertical distributions of $K(z)$ were successfully used to simulate the vertical distribution of phytoplankton biomass, nutrients, and dissolved oxygen for the same area or in similar ecological situations in previous studies [*Zakardjian and Prieur*, 1994; *Varela et al.*, 1992, 1994]. In particular, the depth value of

Table 1. List of Symbols and Values of Parameters Used in the Simulations

	Value	Unit	Description
B	var (z, t)	mmol N m^{-3}	phytoplankton biomass in terms of nitrogen
NO_3	var (z, t)	mmol m^{-3}	nitrate concentration
NH_4	var (z, t)	mmol m^{-3}	ammonia concentration
NO_2	var (z, t)	mmol m^{-3}	nitrite concentration
O_2	var (z, t)	mmol m^{-3}	dissolved oxygen concentration (converted in mL L^{-1})
μ	var (z, t)	d^{-1}	phytoplankton growth rate
t_d	var (z, t)	d	phytoplankton doubling time in nitrogen biomass
S_{NO3}	var (z, t)	dimensionless	fraction of phytoplankton growth sustained by nitrate
S_{NH4}	var (z, t)	dimensionless	fraction of phytoplankton growth sustained by ammonium
S_{NO2}	var (z, t)	dimensionless	fraction of phytoplankton growth sustained by nitrite
$H(B, S_b)$	var (z, t)	dimensionless	Haeviside function associated with the feeding threshold of the Ivlev-type grazing function
BEM	var (t)	mmol N m^{-2} d^{-1}	depth-integrated amount of grazed and nonregenerated nitrogen
F_b	var (t)	mmol N m^{-2} d^{-1}	total nitrogen flux across the bottom boundary
F_s	var (t)	mmol N m^{-2} d^{-1}	total nitrogen flux across the mixed layer lateral boundary
N_t	var (t)	mmol N m^{-2}	total nitrogen amount of the simulated system
t_c	var (z)	d	phytoplankton doubling time in carbon biomass
$\langle E \rangle$	var (z)	Ein m^{-2} d^{-1}	averaged light conditions experienced by the cells during doubling time $t_c(z)$
N	var (z)	s^{-1}	Brunt-Väisälä frequency
ε	var (z)	m^2 s^{-3}	dissipation rate of turbulent kinetic energy
K	var (z)	m^2 d^{-1}	turbulent diffusivity coefficient
W	0–5	m d^{-1}	upward advection velocity
E_0	80.0 Ein m^{-2} d^{-1}		surface irradiance
χ	0.07 m^{-1}		light extinction coefficient
t_{dmin}	0.5 d		minimum phytoplankton doubling time
t_{crit}	8.4 d		maximum phytoplankton doubling time
K_e	10.0 Ein m^{-2} d^{-1}		half-saturation constant for light versus photosynthesis relationship [*Kiefer and Mitchell*, 1983]
K_{NO3}	1.0 mmol m^{-3}		half-saturation constant for the Michaelis-Menten kinetics of nitrate or nitrite uptake [*Eppley et al.*, 1969]
K_{NH4}	0.1 mmol m^{-3}		half saturation constant for the Michaelis-Menten kinetics of ammonia uptake [*Eppley et al.*, 1969]
$\bar{Z}$	1.2 mmol N m^{-3}		mean microzooplankton and mesozooplankton biomass
r_{max}	1.0 d^{-1}		maximum grazing rate for the Ivlev-type function[1]
β	0.75 (mmol N)$^{-1}$ m^3		ingestion coefficient for the Ivlev-type grazing function[1]
S_b	0.05 mmol N m^{-3}		feeding threshold for the Ivlev-type grazing function[1]
R_{1max}	48.0 nmol m^{-3} d^{-1}		maximum oxidation rate for ammonia[2]
R_{2max}	48.0 nmol m^{-3} d^{-1}		maximum oxidation rate for nitrite[2]
K_R	0.07 mmol m^{-3}		half-saturation constant for the ammonia and nitrite oxidation kinetics [*Olson*, 1981]
pq_1	2.0 mol O_2 (mol C)$^{-1}$		photosynthetic quotient for phytoplankton growth sustained by nitrate or nitrite [*Williams et al.*, 1979]
pq_2	1.25 mol O_2 (mol C)$^{-1}$		photosynthetic quotient for phytoplankton growth sustained by ammonia [*Williams et al.*, 1979]
α_1	1.5 mol O_2 (mol N)$^{-1}$		molar ratio for oxygen consumption during ammonia oxidation [*Kaplan*, 1983]
α_2	2.0 mol O_2 (mol N)$^{-1}$		molar ratio for oxygen consumption during nitrite oxidation [*Kaplan*, 1983]
ϕ	10.0 mol O_2 (mol N)$^{-1}$		molar ratio for oxygen consumption during ammonia excretion by zooplankton[3]
PV	2.0 m d^{-1}		piston velocity of the O_2 atmosphere/ocean exchange function
H	10 m		thickness of the imposed upper mixed layer
L			horizontal length scale of the upward motions zone
δt	0.5 h		time step of the Eulerian grid
δz	1.0 m		spatial increment of the Eulerian grid ($\delta z = H = 10$ m for the single upper mixed layer grid point)

Here var denotes variables by opposition to parameters.
[1]Mean values for the Western Mediterranean, e.g., *Andersen and Nival* [1988a, b]. [2]Highest values in the range observed at the sea, e.g., *Kaplan* [1983] and *Ward* [1987]. [3]Mean values in the range from the literature, e.g., *Alcaraz* [1988] and *Small et al.* [1983].

the TKE dissipation rate and consequently of $K(z)$ scales the productivity of the simulated new production system in situations with no upward motion [e.g., *Zakardjian and Prieur*, 1994; *Sharples and Tett*, 1994; *Varela et al.*, 1994; *Moisan and Hofmann*, 1996; *Hood and Olson*, 1996].

The imposed upward advection was constant with depth and varied from 0 to 5 m d^{-1} for six simulations. In keeping with the continuity equation, we modified the numerical scheme and the boundary conditions to allow the upwelled flows to escape laterally throughout the imposed well-mixed layer (see Figure 2 and details in section 2.4). This avoids considering a real two-dimensional domain. Continuity of the advective flow was assumed for a single grid point, which stands for the imposed upper well-mixed layer of $H = 10$ m (Figure 2). We stated that below this upper mixed layer $W \neq 0$ and $U = 0$, while within the upper mixed layer $W = 0$ and $U \neq 0$. Thus the continuity equation gives

$$\frac{W}{H} = \frac{U}{L} \tag{4}$$

where L is the characteristic horizontal length scale of the zone where upward motions occurs. Equivalence in term of a hori-

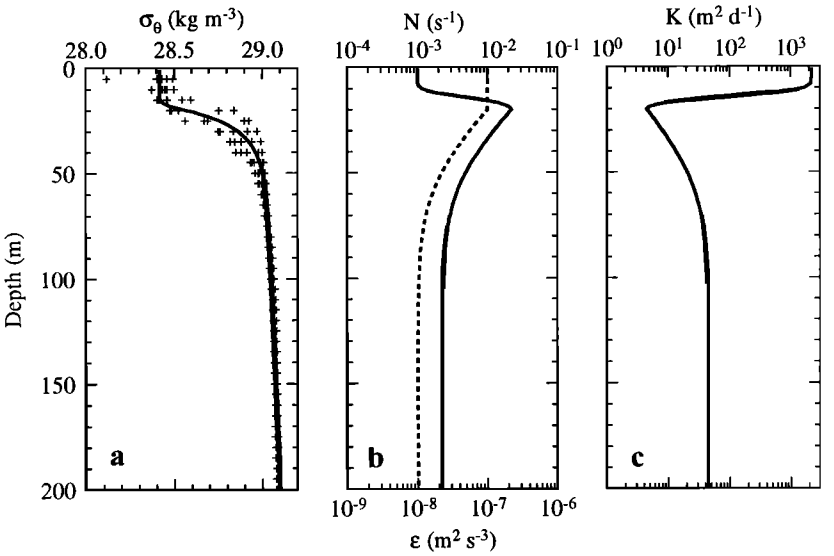

Figure 1. (a) Observed (crosses) and imposed (solid line) potential density excess profiles (σ_θ) and (b) imposed Brunt-Väisälä (N) and turbulent kinetic energy dissipation rate (ε) used to define (c) the turbulent diffusion coefficient (K); observed σ_θ profiles are from conductivity-temperature-depth (CTD) stations PRO60, PRO61, PRO62, PRO79, and PRO80 (Prolig 2 cruise), as representative of typical stratified waters of the central zone of the Ligurian Sea in May.

zontal flow (through (4)) is to be defined with regard to the upward motion zone length scale. This length scale would be approximately equal to or less than the barocline deformation radius L_d which is ~13 km in the Liguro-Provençal front. Taking $L = L_d$ the upper limit for the equivalent horizontal ageostrophic advection (U) ranges between 1.5 cm s^{-1} for $W = 1$ m d^{-1} and 7.5 cm s^{-1} for $W = 5$ m d^{-1}. This range is 1 order of magnitude lower than the primary circulation (0.5–1 m s^{-1}) and may effectively be related to a secondary ageostrophic circulation in a frontal system.

2.3. Phytoplankton Growth Rate

According to *Prieur and Legendre* [1988], the phytoplankton growth rate μ in equations (1.1)–(4) in the appendix is estimated from the longest doubling time between the time $t_c(z)$, which corresponds to the doubling time in terms of carbon

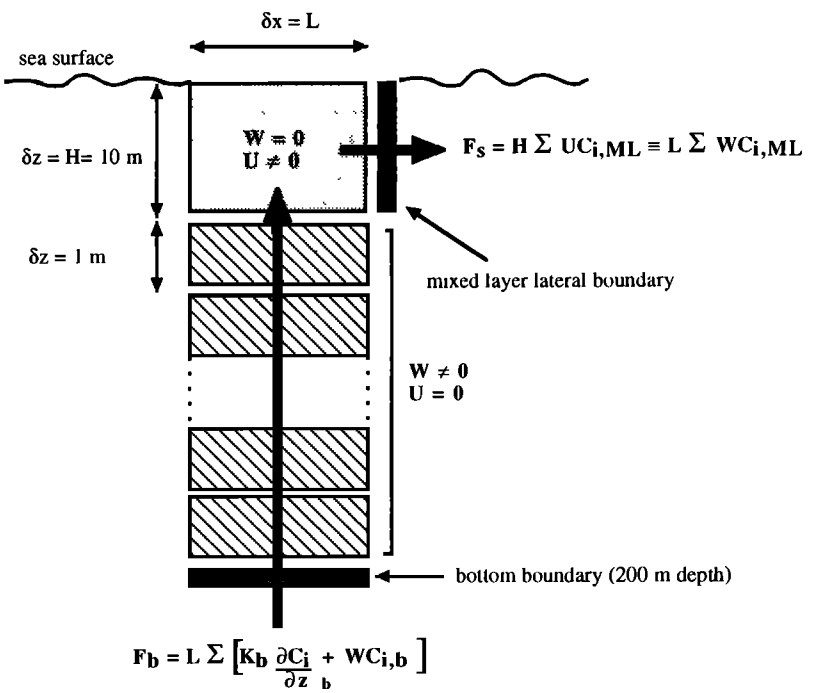

Figure 2. Schematical representation of the numerical grid and the advection processes in the simulated water column.

biomass as the result of light limitation, and the time $t_s(z, t)$, which is the doubling time in terms of nitrogen biomass as a function of nutrient limitation:

$$\mu(z, t) = \frac{\ln (2)}{\max [t_c(z), t_s(z, t)]} \tag{5}$$

$$t_c(z) = t_{dmin}\left[1 + \frac{K_e}{\langle E \rangle}\right] \tag{6}$$

$$t_s(z, t) = \frac{t_{dmin}}{f[N]} \tag{7}$$

where $\langle E \rangle$ is the average light received by the cells during their doubling time $t_c(z)$ and $f[N]$ is a term for nitrogen limitation estimated from the nutrient conditions at depth z and time t. The light conditions were defined with a surface photosynthetically available light of 80 Ein m^{-2} d^{-1}, which is representative of late spring conditions in the Western Mediterranean and with a diffuse attenuation coefficient $\chi = 0.07$ m^{-1}, a typical value for Mediterranean offshore waters (L. Prieur, unpublished data, 1972). The photosynthetically available radiation (PAR) is distributed equally on a 24 hours basis. The depth of the euphotic layer (i.e., 1% of surface PAR) is 66 m. The formulation of the doubling time $t_c(z)$ takes into account vertical motions of the phytoplankton cells in the light field as described later in this section. Vertical motions previously experienced by phytoplankton at depth z during a time scale ΔT can be numerically computed from the following implicit equation:

$$\Delta T = \int_z^{z'(\Delta T)} \frac{1}{W}\,\delta z \tag{8}$$

This equation means that cells were advected from depth $z'(\Delta T)$ to z during ΔT(z positive with depth). Implicit (8) was solved numerically for the couple (z, z') with an iterative procedure and tabulated for ΔT = 0–9 days. Knowing the spatial domain explored by the cells between time $t = 0$ to $t = t_c(z)$, the averaged irradiance $\langle E \rangle$ was numerically computed from

$$\langle E \rangle = \frac{1}{t_c(z)} \int_0^{t_c(z)} E_0 \exp [-\chi z'(t)]\delta t \tag{9}$$

and the system of implicit (6) and (9), which links $t_c(z)$ and $\langle E \rangle$, was solved numerically by an iterative method. The term $f[N]$ used in (7) to estimate the doubling time in nitrogen biomass $t_s(z, t)$ was computed from the substitutional model of *O'Neill et al.* [1989] as

$$f[N] = \frac{[NO_3 + NO_2]K_{NH4} + NH_4K_{NO3}}{K_{NH4}K_{NO3} + [NO_3 + NO_2]K_{NH4} + NH_4K_{NO3}} \tag{10}$$

where K_{NO3} and K_{NH4} are different half-saturation constants for uptake of nitrate-nitrite and ammonia, respectively, so that if $K_{NO3} \gg K_{NH4}$, ammonia can be taken up preferentially rather than nitrate or nitrite [*McCarthy*, 1980; *Dortch*, 1990]. In addition, we assumed no phytoplankton production ($\mu = 0$) for doubling times greater than t_{crit} = 8.4 d [*Richardson et al.*, 1983]. Phytoplankton assimilation of the three nitrogen sources in A2–A4 were calculated as the products of $\mu(z, t)$ (computed from time $t_s(z, t)$ or $t_c(z)$) and the S_i ratios (i stands for one nitrogen-nutrient source), which resulted from the partitioning of the upper term of $f[N]$. For example, using NH_4 as an illustration,

$$S_{NH4} = \frac{NH_4K_{NO3}}{[NO_3 + NO_2]K_{NH4} + NH_4K_{NO3} + K_{NH4}K_{NO3}} \tag{11}$$

2.4. Numerical Techniques: Boundary and Initial Conditions

The model extends vertically to a depth of 200 m, and z is positive in the downward direction. Except for the mixed layer grid point, A1–A5 were rewritten in semi-implicit Crank-Nicolson discrete forms using a backward scheme for the advection term and a control volume approach derived scheme for the diffusion term [see *Roach*, 1972]. According to Figure 2, the imposed mixed layer suffers an upward advective flux WC_1, which escapes through a lateral advective flow UC_{ML}, where subscripts ML and 1 denote mixed layer and submixed layer conditions, respectively (see Figure 2). For the mixed layer grid point, the discrete scheme for advection can be written as

$$\frac{\partial WC}{\partial z} + \frac{\partial UC}{\partial x} \approx \frac{WC_1}{H} - \frac{UC_{ML}}{L} \tag{12}$$

Taking into account (4), this scheme can be simplified to a scheme similar to the underlying grid points except that $\delta z = H$. The boundary conditions at the surface and at the mixed layer lateral boundary are no diffusive fluxes (spatial derivatives set to zero for all variables). Then, the numerical scheme for the vertical diffusion terms are not changed except for the distance used for the computation of vertical gradients between the mixed layer grid point and the first underlying grid point:

$$\frac{\partial C}{\partial z} \approx \frac{(C_1 - C_{ML})}{(H + \delta z)/2} \tag{13}$$

We assumed boundary conditions at the bottom (200 m depth) to be an infinite and homogeneous layer with time independent concentrations for all variables. The fixed concentrations at this bottom boundary were set to 8.0 mmol m^{-3} for NO_3, 200 mmol m^{-3} (4.5 mL L^{-1}) for dissolved oxygen, and zero for phytoplankton biomass, NO_2, and NH_4. To check the temporal evolution of the total nitrogen in the system, nitrogen mass fluxes across the lateral mixed layer boundary (F_s) and the bottom boundary (F_b) were computed during the simulation as

$$F_b = L \sum \left[K_b \left.\frac{\partial C_i}{\partial z}\right|_b + WC_{i,b}\right] \tag{14}$$

$$F_s = H \sum UC_{i,ML} \equiv L \sum WC_{i,ML} \tag{15}$$

where subscript b denotes bottom conditions and subscript i stands for each nitrogen variable (phytoplankton biomass, NO_3, NH_4, and NO_2). Note that the term L steps in the expression for BEM, F_s, and F_b in a similar way and can be omitted in the computation, as U. A posteriori estimates for U and L can be made in view of observations at the sea (see section 2.2).

In order to test the convergence of the final solutions, we used two sets of initial conditions. The first set (hereafter Set I) was chosen to be representative of late winter conditions in the Western Mediterranean, where initial nitrate concentrations were set to 8.0 mmol m^{-3} for the whole water column

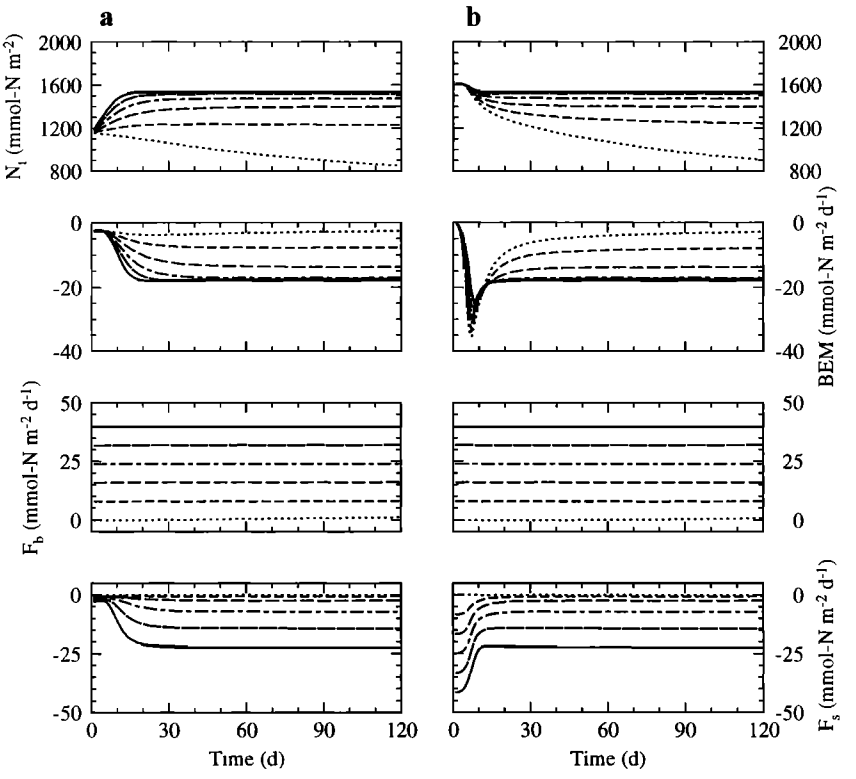

Figure 3. Time evolutions of total nitrogen (N_t), biologically exported mater (BEM), nitrogen bottom flux (F_b), and nitrogen surface flux (F_s) from the simulations with initial conditions (a) Set I and (b) Set II. Incoming and outcoming fluxes have positive and negative values, respectively. The light-dotted and continuous lines are for $W = 0$ and $W = 5$ m d^{-1}, respectively; the dotted-dashed lines are darkened as W increases from 1 to 4 m d^{-1}. Note that the three nitrogen mass fluxes (three bottom regions) equilibrate themselves at steady state and that the steady-state is independant of the initial conditions.

and phytoplankton biomass, nitrite, and ammonia were set to 0.1 mmol m^{-3} in the euphotic zone while zero below. The initial dissolved oxygen concentrations were set to 245 mmol m^{-3} (a saturated value for surface temperature and salinity of 15.5°C and 38.4 practical salinity unit (PSU), respectively) in the upper well-mixed layer and, below this, were set to the bottom concentrations. The second set of initial conditions (Set II) defined an initially nutrient-impoverished euphotic zone (NO_3, NO_2, and NH_4 set to 0.1 mmol m^{-3}) with a phytoplankton biomass of 0.5 mmol N m^{-3} and supersaturated dissolved oxygen concentrations (110% or 270 mmol m^{-3}). Below the euphotic zone, initial concentrations were the same as bottom boundary concentrations. The system of discrete equations was then solved numerically with the method described by *Zakardjian and Prieur* [1994] for a time step δt = 0.5 h and a spatial increment δz = 1 m below the well-mixed layer and $\delta z = H = 10$ m for the well-mixed layer grid point.

3. Numerical Results

3.1. Steady State and Vertical Distributions of Scalar Variables

Figure 3 shows the evolution of the total nitrogen (N_t), the exported nitrogen (BEM) and the advective-diffusive fluxes of nitrogen at the bottom boundary (F_b) and through the upper mixed layer lateral boundary (F_s). Changes in total nitrogen during the simulation depended on the balancing of the two nitrogen boundary fluxes and biologically exported matter and led to steady states, which were independent of the initial conditions used. Running the model without vertical advection gave a steady state solution after 120 days of simulation. The time needed to achieve the steady state was significantly reduced as the advection velocity was raised. It was 60 days for $W = 1$ m d^{-1} and reduced to less than 20 days for $W = 5$ m d^{-1}. The vertical distribution of all scalars was also steady and independent of the initial conditions when the steady state for total nitrogen was achieved. As discussed by *Zakardjian and Prieur* [1994], this time evolution of the simulated ecosystems shows two phases. The first and rapid reaction phase led to the setting up of the primary production system and is particularly apparent with initial conditions of Set I. The longer second phase led to the equilibrium of the three nitrogen mass fluxes (BEM, F_s and F_b). This second and so-called relaxation phase is predominant for the time needed to achieve the steady state and is mainly a function of the rate of the nitrogen loss, i.e., the BEM in our model when $W = 0$. For nonzero upward advection, the upwelled waters escaped through the mixed layer lateral boundary, carrying along inorganic (NO_3, NO_2, and NH_4) and organic (B) nitrogen. It acted as the BEM and, then, reduced the time needed to achieve the steady state.

The steady state vertical distributions obtained with the reference simulation ($W = 0$) show characteristic features of a LTR-type phytoplankton-nutrient system that is representative of a stratified water column for late spring conditions in the Western Mediterranean (Figure 4). The upper layer is nutrient-impoverished, and a deep maximum of phytoplankton bio-

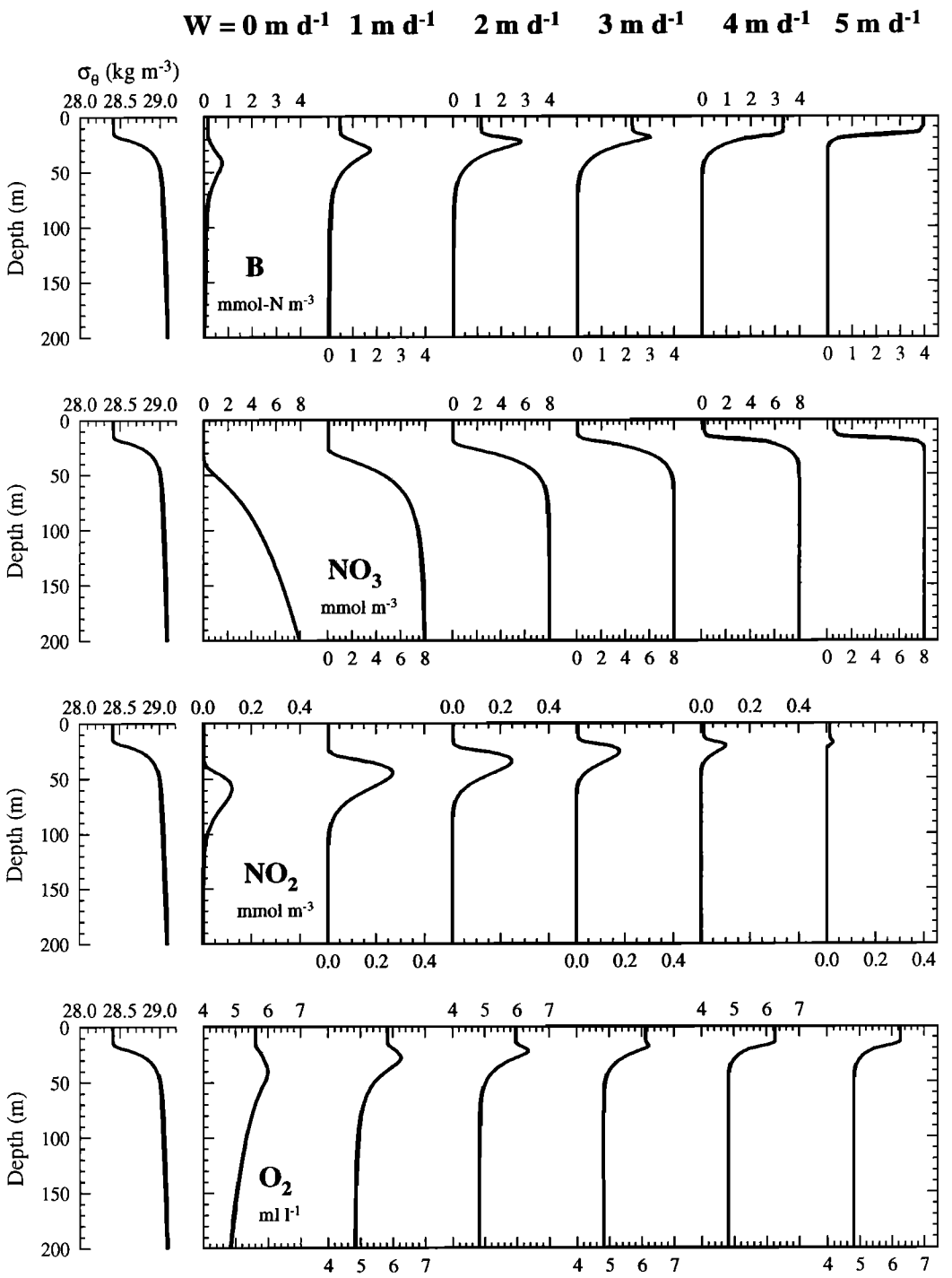

Figure 4. Potential density excess (σ_θ, left) and steady state vertical distribution of phytoplankton biomass (B), nitrate (NO_3), nitrite (NO_2), and dissolved oxygen (O_2) with increasing upward advection (W). Note the shoaling of the nitracline and maxima of phytoplankton biomass, NO_2, and O_2 toward the surface for increasing W.

mass (hereafter DBM) of ~0.8 mmol N m^{-3} is present at the top of the nitracline (45 m depth). The vertical distribution of dissolved oxygen shows saturated values in the upper well-mixed layer and a broad and over-saturated maximum ($O_2 \approx$ 6.2 mL L^{-1}) extending from the top of the pycnocline to the DBM. A slight nitrite maximum (0.15 mmol m^{-3}) was simulated 20 m deeper than the biomass maximum.

The upward advection affected the steady state vertical distribution as seen in Figure 4. First, one notes the shallowing of the nitracline, the DBM, and the O_2 maximum for low upward advections ($W \leq 3$ m d^{-1}). The nitracline and DBM shoaled to 30 and 20 m when W was set to 1 and 3 m d^{-1}, respectively. The broad dissolved oxygen maximum at depth became progressively shallower as W was raised while the oxycline remained at the same depth as the nitracline. Nitrate concentrations were always extremely low above the DBM, so that all the

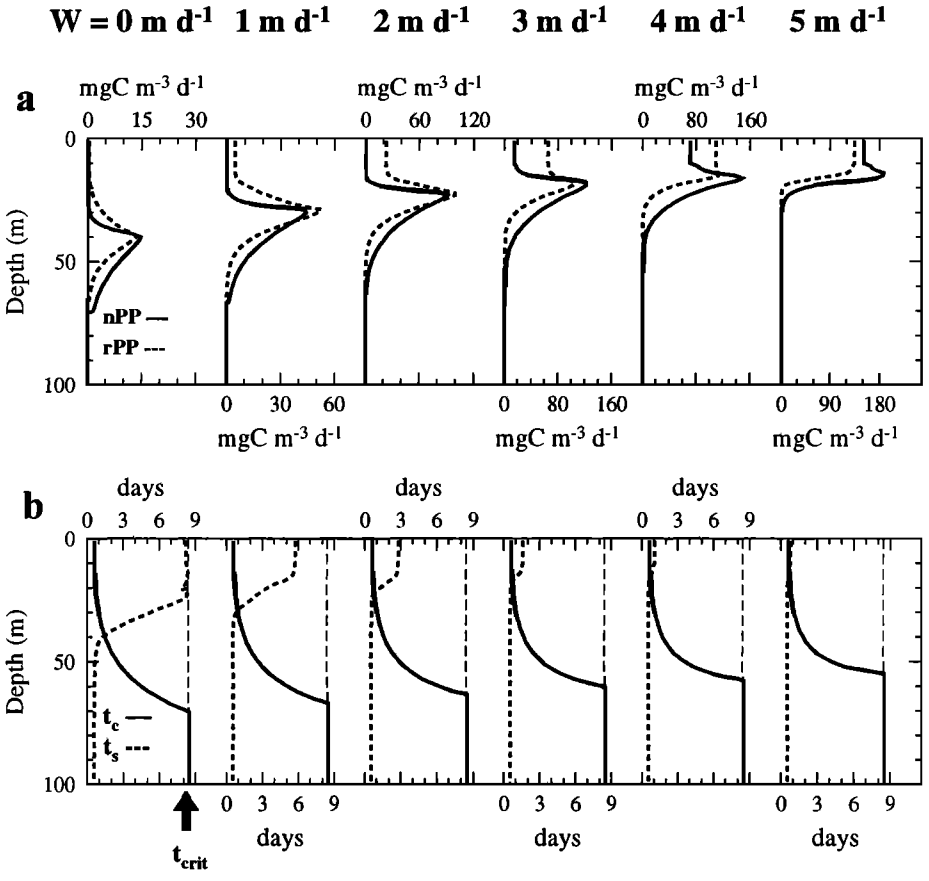

Figure 5. (a) Steady state vertical distribution for primary production rates and (b) doubling times for increasing upward advections (W). Dotted and solid lines are for regenerated and new production, respectively, and $t_s(z, t)$ and $t_c(z)$, respectively. Abscissa units for primary production are changed as primary production rates dramatically increased for increasing W. Doubling times greater than t_{crit} = 8.4 d, which indicate no growth due to either nitrogen ($t_s(z, t)$) or light ($t_c(z)$) limitation, are fixed to 8.5 d on graphs.

LTR characteristics were shallowed with increasing W. Furthermore, the phytoplankton biomass increased with upward advection, reaching a maximum value of 3 mmol N m^{-3} at the DBM and 2.2 mmol N m^{-3} in the upper well-mixed layer for W = 3 m d^{-1}. The nitracline, DBM, and deep O_2 maximum were progressively sharpened as they approached the upper pycnocline. Under conditions of moderate upward advection ($W \approx$ 1–2 m d^{-1}), the NO_2 deep maximum was shallower, as found for the nitracline and biomass and O_2 maxima, and increased to 0.3 mmol m^{-3}.

Second, there was an alteration of the LTR characteristics when W was set to 4–5 m d^{-1}. The phytoplankton biomass was homogeneous with depth above the pycnocline and rapidly decreased below the top few meters of the pycnocline. The nitracline and oxycline were at the same depth as the upper pycnocline, while the deep nitrite maximum rapidly decreased. Such features have been described as a HTR-type situation, which reveals another system of new production [*Zakardjian and Prieur*, 1994]. The phytoplankton biomass increased in the upper mixed layer, up to 3.4 mmol N m^{-3} when W = 5 m d^{-1}, while NO_3 concentrations were ~0.5–1.0 mmol m^{-3}. Oxygen consistently remained at slightly supersaturated values (105%) in the upper mixed layer. Ammonia vertical distributions are not described because no data were available to make comparisons with the simulations. Nevertheless, we verified that NH_4 concentrations were always lower than NO_2 concentrations, and that its vertical distribution did not show any significant or additional structure.

3.2. Vertical Distribution of Primary Production

Figure 5a shows the vertical distribution of new and regenerated production at steady state. A deep maximum of new production was always found at the same depth as the nitracline and the DBM, when the latter was present. The maximum for new production at depth was ~15 mg C m^{-3} d^{-1} for W = 0 and continuously increased as W was raised, reaching 165 mg C m^{-3} d^{-1} when W = 5 m d^{-1}. Only in simulations when $W \geq$ 3 m d^{-1} did significant new production rates (20–150 mg C m^{-3} d^{-1}) occur in the upper well-mixed layer. Moreover, for W in the range of 4–5 m d^{-1}, the deep maximum for new production found just above the top of the pycnocline was then clearly disconnected from the homogeneous phytoplankton biomass in the upper layer. Such a spatial uncoupling of phytoplankton biomass and the vertical distribution of new production was described as another characteristic feature of the HTR new production system [*Zakardjian and Prieur*, 1994]. For the reference simulation and low upward advection (W = 1–3 m d^{-1}), the distribution of regenerated production in response to upward advection showed similar features to that of new production. The model produced a deep maximum for regenerated production that followed the shallowing of the DBM (Figure 5a). The regenerated produc-

tion at depth increased, as did the new production, from 17 mg C m^{-3} d^{-1} for $W = 0$ to a maximum value of 100 mg C m^{-3} d^{-1}. For higher advection velocities ($W > 3$ m d^{-1}), the regenerated production, along with the phytoplankton biomass, was confined to the upper mixed layer and did not show any deep maximum by contrast with new production. Regenerated production rates were 100–120 mg C m^{-3} d^{-1}, and the proportion of regenerated production to total production decreased slightly. Maximum total primary production rates reached 280 mg C m^{-3} d^{-1} for $W = 5$ m d^{-1}. This value is in the lower range of primary production rates for coastal upwelling conditions, which can be as high as 300–600 mg C m^{-3} d^{-1} [*Small and Menzies*, 1981; *Jones and Halpern*, 1981].

3.3. Effect of Upward Advection on Phytoplankton Doubling Times

The vertical distribution of doubling times $t_c(z)$ and $t_s(z, t)$ (Figure 5b) gave information on how the upward advection affects the vertical distribution of primary production. For the reference situation ($W = 0$), which illustrates the LTR new production system, the water column was partitioned in an upper nitrogen-limited layer, where phytoplankton growth depended on $t_s(z, t)$, and a deeper light-limited layer, where phytoplankton growth rate was related to $t_c(z)$. The change from light limitation to nitrogen limitation occurred in the top few meters of the nitracline and led to the deep maximum for new production at the depth where $t_c(z) = t_s(z, t)$. The development of this LTR new production system is related to the depth interval between the $K(z)$ minimum and the bottom of the euphotic layer, where the phytoplankton biomass traps the upward nitrate flux and limits the nutrient replenishment of the upper layer. As a consequence, $t_s(z, t)$ strongly increases just above the DBM and confines new production to the deepest part of the photic zone. The coupling of a deep new production maximum with the upper nitracline, the DBM, and the deep O_2 maximum is a characteristic feature of the LTR new production system [*Zakardjian and Prieur*, 1994].

The main effect of upward advection was to shallow the depth where the nitrate upward flux is balanced by the phytoplankton assimilation. This is illustrated by the shallowing of the layer where $t_s(z, t)$ increased, the lower values of $t_s(z, t)$ in the upper well-mixed layer (Figure 5b), as the indication of less nutrient limitation and by the increase in the biomass needed to trap the nitrate upward flux (Figure 4). As the doubling times $t_s(z, t)$ decrease, the primary production rates increase. For upward advections >3 m d^{-1}, phytoplankton growth was only slightly nitrogen-limited in the upper mixed layer ($t_s(z, t) < 1$ d). This agreed with higher nitrate concentrations, ~0.5 mmol m^{-3} and greater, and significant new production rates observed in the upper layer for the same simulations.

Otherwise, upward advection reduced the "productive zone," that is, the upper layer where phytoplankton cells receive sufficient amounts of light for growth. According to the formulation for $t_c(z)$ (see (6) and (8)–(9)), phytoplankton at depth z, which are subjected to an upward advection, must come from the deeper layers and thus have experienced lower irradiance than at the fixed depth z. This means that moderate upward advection modifies the light conditions as "seen" by the phytoplankton cells during their doubling time in reference to the imposed light field. The timescale for advection through one optical depth is $t_{om} = 1/W\chi$, and, for $\chi = 0.07$ m^{-1}, it ranges from 14 days for $W = 1$ m d^{-1} to 2.8 days for $W = 5$ m d^{-1}. This range of t_{om} values indicates that the effect of upward advection on light limitation for growth is significant at the bottom of the euphotic layer, i.e., when $t_c(z) > t_{om}$. In these simulations, an equivalent of the compensation depth is defined through the critical time $t_{crit} = 8.4$ d (see section 2.3). The depth where $t_c(z) = t_{crit}$, which indicates definitive light limitation for growth, shallowed from 70 m when $W = 0$ to 54 m and when $W = 5$ m d^{-1} (Figure 5b). By limiting the depth of the euphotic zone as seen by the phytoplankton cells, the upward advection furthered the shallowing of the LTR characteristics.

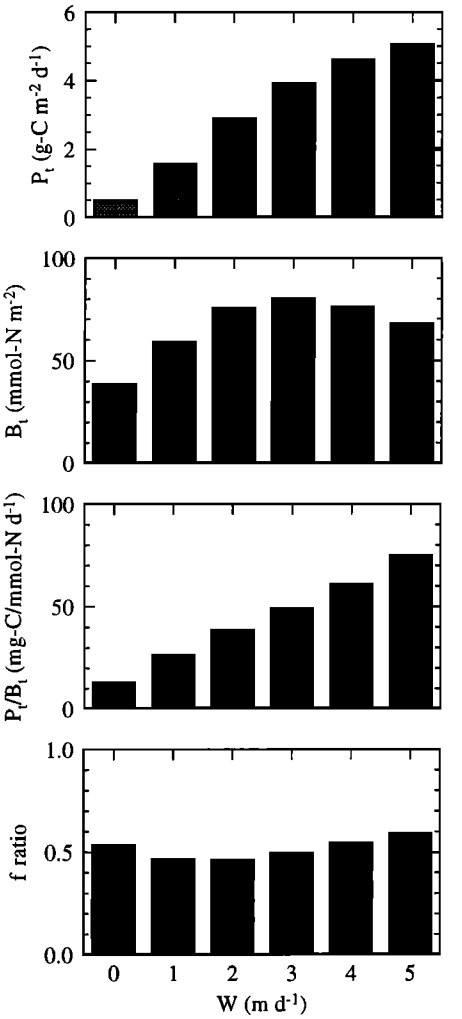

Figure 6. Depth-integrated (0–200 m) phytoplankton biomass (B_t), depth-integrated total production (P_t), depth-integrated assimilation ratio (P_t/B_t) and depth-integrated f ratio at steady state for increasing upward advections (W).

3.4. Effects of Upward Advection on the Productivity Indexes of the Water Column

The steady state, depth-integrated primary production (new plus regenerated production), phytoplankton biomass and f ratio, i.e., depth-integrated new production versus total production [*Eppley and Peterson*, 1979], are showed in Figure 6. For low-advection velocities ($W = 1$–3 m d^{-1}) the depth-integrated phytoplankton biomass and primary production increased, following the higher nutrient enrichment of the euphotic zone. When the upward advection was set to 4–5 m d^{-1},

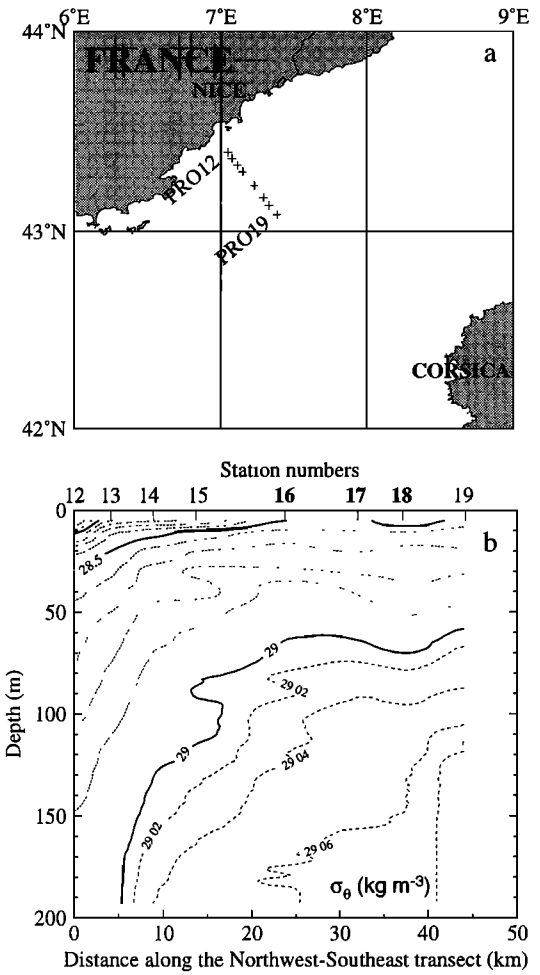

Figure 7. (a) Locations of THES transect PRO12–PRO19 (May 18, 1985) conducted across the Liguro-Provençal front during the Prolig 2 cruise, and (b) potential density excess (σ_θ) along the same THES transect. As two CTDs were mounted on the THES system during this transect, we were able to verify that density inversions near 40 and 90 m depth for station PRO15 were not due to technical artifacts; at present, this particular feature has not been clearly elucidated.

the depth-integrated primary production still increased while the biomass decreased significantly. As a result, the depth-integrated production versus phytoplankton biomass continuously increased with increasing upward advection, from 15 mg C (mmol N)$^{-1}$ d^{-1} for $W = 0$ to 75 mg C (mmol N)$^{-1}$ d^{-1} for $W = 5$ m d^{-1}. These changes in the depth-integrated assimilation ratio of the water column are related to the fate of the phytoplankton biomass due to the upward advection. The increase in phytoplankton biomass in the upper mixed layer for $W > 2$ m d^{-1} (Figure 4) indicated that a significant amount of the biomass produced locally by the increased new production was advected throughout the upper mixed layer and rapidly carried out of the local water column. Furthermore, as the thickness of the biomass-rich layer decreased for $W \geq 3$ m d^{-1} (Figure 4), the depth-integrated biomass continuously decreased for higher-upward advections (Figure 6).

The depth-integrated f ratio showed only slight changes in the six simulations. For the reference simulation ($W = 0$), it was ~0.55, a value representative of late spring bloom conditions in the north Western Mediterranean. It slightly decreased to 0.45 for low-upward advection (1–2 m d^{-1}) and showed its higher value of ~0.6 for the highest-upward advection. In this model, the source of regenerated nutrients was directly linked with the concentration of biomass at depth through the grazing function (see A3). The slight decrease in the f ratio for low-upward advection can be explained by a greater retention of regenerated nitrogen in the euphotic layer due to a reduced deep mixing of phytoplankton biomass. For higher-upward advection, an increased amount of regenerated nutrients were advected throughout the mixed layer, as the phytoplankton biomass, leading to a relative decrease in regenerated production as a proportion of total production.

4. Comparisons With Observations

4.1. THES Data in the Liguro-Provençal Front

During the Prolig 2 cruise (May–June 1985), we used a towed hydroelectric system (THES) to evaluate the possible influence of vertical advective and turbulent motions on the spatial distribution of variables involved in primary production in the Liguro-Provençal front. The prototype THES has been previously described by *Prieur* [1985] and *Prieur et al.* [1993]. The THES provides simultaneous and quasi-continuous measurements of physical parameters (pressure, temperature, and conductivity) and biological variables (in vivo Chl *a* fluorescence, nutrients, dissolved oxygen, pH, and pCO_2) with a spatial resolution of 0.3 m down to 200 m depth for vertical profiles or 50 m for horizontal transects. In this section we will present vertical distributions from three THES stations (PRO16, PRO17, and PRO18), which show similar features when compared with the simulations described in section 3. The positions of the three stations along with the underlying density structure are shown in Figure 7. Stations PRO18 and PRO17 were outside of the frontal structure, on the heavy side of the density gradient, while station PRO16 was just inside the limit of the front (Figure 7b). Vertical profiles from stations further than the frontal zone (stations 12–15) are not described here because they show special patterns (such as double maxima of Chl *a* and NO_2 and localized minima/maxima for O_2 and NO_3 at depth), which may be the results of oblique, sheared downward/upward motions. Such complex motions cannot be simulated in a quasi-vertical one-dimensional model.

Except for the higher pigment concentrations (Chl $a \approx 0.5$ mg m^{-3}) in the upper 30 m, the vertical distributions of Chl *a*, NO_3, and O_2 at station PRO18 (Figure 8) showed similar patterns to the reference simulation (Figure 4, $W = 0$). A deep Chl *a* maximum (hereafter DCM) of ~0.8 mg Chl *a* m^{-3} was found at a depth of 50 m. The upper layer was nutrient depleted and the nitracline was in the vicinity of the DCM. The vertical distribution of dissolved oxygen displayed supersaturated values (110%) at the sea surface (~6.0 mL L^{-1}) and a broad maximum (5.9 mL L^{-1} $\leq O_2 \leq$ 6.05 mL L^{-1}) that extended from a depth of 15 m to the upper part of the nitracline. Below this depth, O_2 concentrations decreased slightly to a nearly constant value of ~4.8 mL L^{-1} at 150 m deep. Concentrations of NO_2 were very low in the surface layer and at depth but showed a deep maximum of ~1.0 mmol m^{-3} 15 m deeper than the DCM. By comparison, stations PRO17 and PRO16 showed similar but shallower and more marked patterns. For station PRO17 (Figure 8), the DCM was near 36 m and reached 1.0 mg m^{-3}. The nitracline and maximum NO_2 concentration (1.18 mmol m^{-3}) were near 36 m and 53 m,

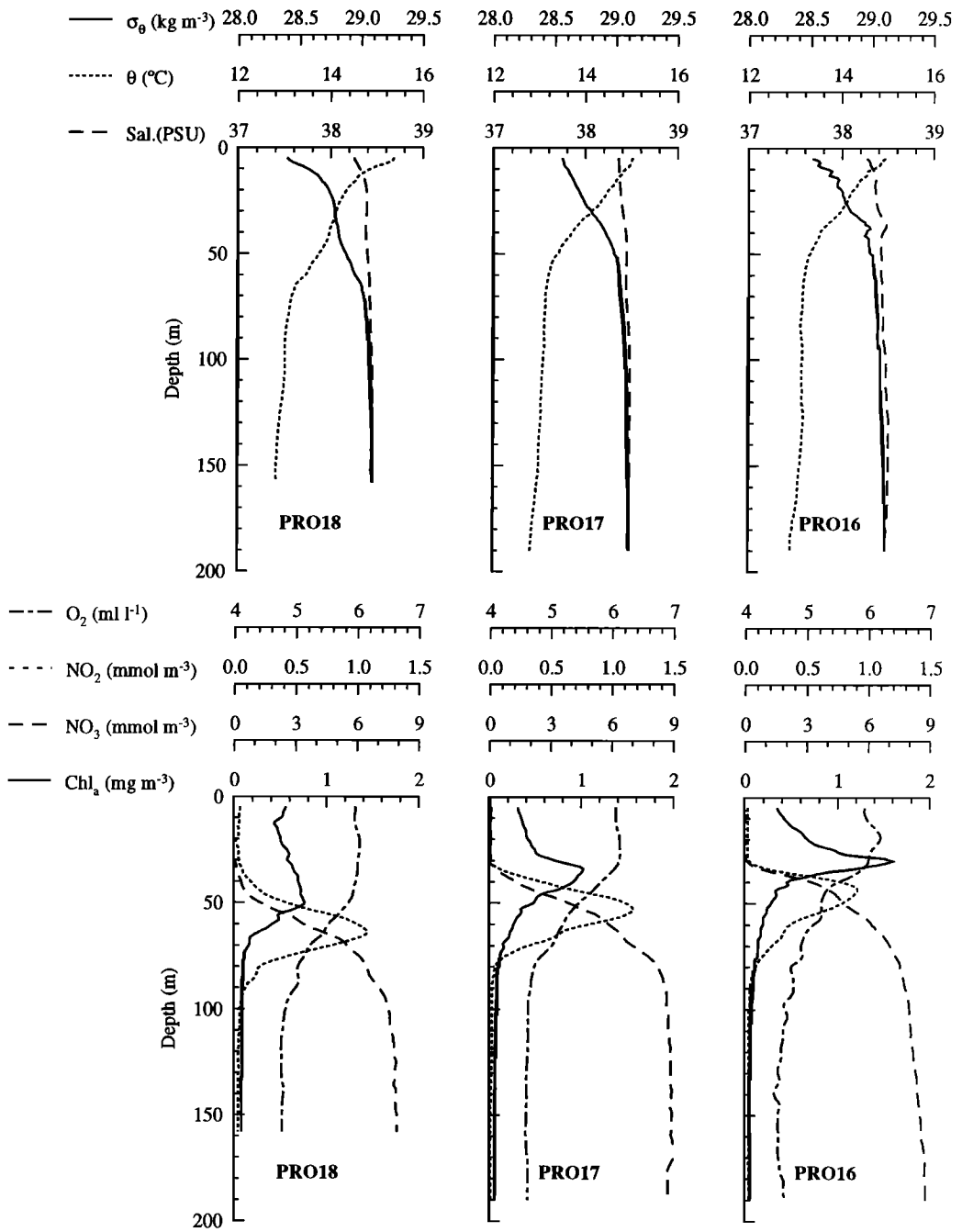

Figure 8. Vertical distribution of potential temperature (θ), salinity (Sal.), potential density excess (σ_θ), chlorophyll *a* (Chl *a*), nitrate (NO_3), nitrite (NO_2), and dissolved oxygen (O_2) for THES stations PRO16–18.

respectively. The surface layer contained slightly higher O_2 concentrations than at station PRO18, ~6.06 mL L^{-1} or 112% of saturation. The O_2 subsurface maximum was also higher ($O_2 \geq 6.15$ mL L^{-1}) and was again depth-limited by the upper nitracline. The O_2 concentration at depth was lower than at station PRO18 (4.60 mL L^{-1} at 150 m). Station PRO16 (Figure 8) showed the shallowest nitracline, oxycline, and deep maxima for Chl *a* and NO_2. The DCM was near 30 m, always in the vicinity of the upper part of the nitracline (33 m depth), and reached two-fold higher concentrations (1.6 mg m^{-3}) than station PRO18. The deep maximum for nitrite was near 43 m depth, which was 10 m deeper than the Chl *a* maximum and showed slightly lower NO_2 concentrations (0.90 mmol m^{-3}) when compared with station PRO17. The dissolved oxygen concentrations were ~6.05 mL L^{-1} (110% of saturation) in the surface layer and 6.05–6.2 mL L^{-1} in the subsurface maximum. The depth of the oxycline was again in the vicinity of the nitracline and the Chl *a* maximum. Oxygen concentration at depth was significantly lower than at station PRO18 and PRO17 (4.53 mL L^{-1} near 150 m).

In an analogy with the results of our simulations, the shallower and sharpened nitracline and Chl *a* and O_2 maxima at stations PRO16 and PRO17 with regards to station PRO18 (Figure 8) may be interpreted as resulting from low-upward advection (W = 1–2 m d^{-1}, see Figure 4) at these two stations. The doubling of the maximum Chl *a* concentration from

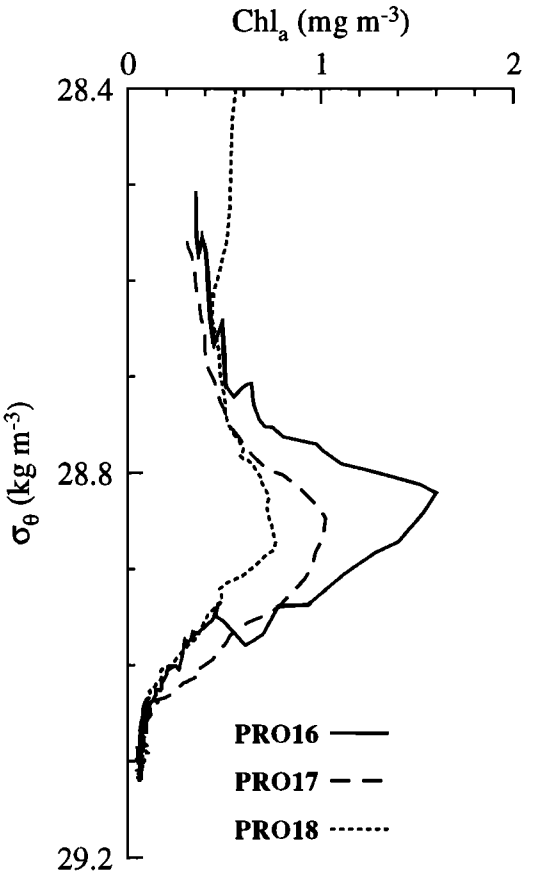

Figure 9. Chlorophyll *a* (Chl *a*) concentrations with potential density excess (σ_θ) as the ordinate from THES stations PRO16–18.

station PRO18 to PRO16 may also support the assumption of such upward motions at station PRO17 and PRO16 even if depth variations of the Chl *a* versus carbon and nitrogen biomass ratios has long been identified as a problem when estimating the phytoplankton biomass from Chl *a* data [*Cullen*, 1981; *Longhurst and Harrison*, 1989]. In fact, both ratios vary strongly according to the light and the nutrient histories of the phytoplankton population [*Laws and Bannister*, 1980; *Falkowski et al.*, 1985; *Claustre and Gostan*, 1987] as well as from its specific composition [*Claustre and Gostan*, 1987; *Claustre et al.*, 1994b]. Nonetheless, the main trend remains that the Chl *a* versus phytoplankton biomass ratio would increase with depth due to photoadaptation, so that a doubling of the Chl *a* concentration when the deep Chl *a* maxima is shallowed is more likely to reflect an increase in phytoplankton biomass. Despite the high maximum rates of ammonia oxidation used (Table 1), the low-simulated NO_2 concentrations (0.15–0.30 mmol m^{-3}) contrasted with the high values (0.9–1.2 mmol m^{-3}) in the THES data. Although the origin of the high-NO_2 concentrations in the THES data can not be explained at this time, such a discrepancy can be accounted for. In natural conditions, nitrite excretion by the phytoplankton biomass in conditions of high nitrate enrichment can account for a large part of the deep NO_2 maximum [*Wada and Hattori*, 1971; *Collos*, 1982; *Collos and Slawyk*, 1983]. This process is not taken into account in the simulations, and it is likely that ammonia oxidation cannot be the unique process to be considered in the Prolig 2 nitrite distributions. Nevertheless, the increased NO_2 concentrations in the simulation with low-upward advection agreed with the hypothesis of moderate upward motion at station PRO17. By comparison, the slightly decreased NO_2 concentration at station PRO16 may show the results of higher-upward motions than for station PRO17, in agreement with the other biochemical variables and the simulations (Figure 4).

In addition to upward advection, several other physical processes may affect vertical distributions of phytoplankton biomass, dissolved oxygen, and nutrients, such as different light conditions, an increase in turbulent mixing at depth [*Varela et al.*, 1992; *Zakardjian and Prieur*, 1994], or internal waves [*Fasham and Pugh*, 1976; *Pingree and Mardell*, 1985]. Internal waves are weak in the north Western Mediterranean Sea and are not likely to account for 20 m depth variations of the Chl *a* maximum. Moreover, the deep Chl *a* maxima of the three THES stations are not on the same isopycnal (Figure 9). Although this density difference is weak (~0.06 kg m^{-3} between station PRO16 and PRO18), Chl *a* concentrations show twofold variations on isopycnals, a feature which is not compatible with being the result of the sole effect of internal waves. Increasing the turbulent mixing at depth, through the TKE dissipation rate for example (see (1)), can lead to a shallowing of the nitracline, the deep Chl *a*, and O_2 maxima and to an increase in the biomass level in response to the higher nitrate supply in the photic zone [*Varela et al.*, 1992; *Zakardjian and Prieur*, 1994; *Moisan and Hofmann*, 1996]. However, high values of the eddy diffusivity affect the shapes of the nitracline and Chl *a* maximum in a contrasted way with the sharpening of the observed nitraclines and vertical distributions of Chl *a* at station PRO16 and PRO17 [e.g., *Moisan and Hofmann*, 1996]. Likewise, changes in the stratification of the water columns between station PRO18 and PRO16 and 17 are not likely to explain the depth-variability of the nitracline and maxima of Chl *a* and O_2. The density field is almost horizontal between station PRO19 and PRO16 despite slight variation of the isopycnal depths (Figure 7). The temperature-salinity diagrams of these stations do not exhibit strong differences, despite of some variations at fixed depth as evidenced on Figure 8. At last, the three THES stations were not spaced far apart (<15 km, see Figure 7) and were investigated in a short time (<6 hours), so that variations in the daily surface irradiance between the three stations can be excluded. In offshore waters, the main factor which would affect the light penetration at depth is the pigment content of the water column [e.g., *Prieur and Sathyendranath*, 1981]. Using the averaged diffuse attenuation coefficient for sea water and Chl *a* given by *Morel* [1988], we estimated the light attenuation due to Chl *a* for the three THES stations (Figure 10). The depth for the 1% light level, which classically defines the depth limit for the euphotic zone, was not significantly different between the three THES stations. This was because the higher Chl *a* concentrations at stations PRO16 and PRO17 did not extend over a sufficient depth interval to affect the light penetration at depth. Thus changes in the light conditions cannot be invoked to explain the changes in the vertical distribution of Chl *a*, nutrients, and dissolved oxygen from the THES data.

Upward advections appeared then to be a good candidate to account for the differences in the vertical distribution of Chl *a*, NO_3, and O_2 from stations PRO18, PRO16, and PRO17. Furthermore, the subsurface temperature and salinity contrast between stations PRO16 and PRO17 and the other stations of the transect (Figure 11) may corroborate the hypothesis of

upward motions at these two stations. In addition, both stations PRO16 and PRO17 show greater values for NO_3 and salinity and lower O_2 concentrations at depth than at station PRO18 (Figure 8). This indicates the intrusion of a deep water mass at those two stations and strengthens the hypothesis of an upwelled flow.

4.2. Primary Production Measurements in Permanent Geostrophic Fronts of the Western Mediterranean

Unfortunately, primary production was not measured during the Prolig 2 cruise, and thus computed primary production will be compared here to primary production measurements conducted in the Almería-Oran front during the Almofront 1 cruise (May 1992) and by *Hecq et al.* [1986] for productivity values off the corsican part of the Ligurian Current. Although the Almería-Oran frontal structure differs slightly from the Liguro-Provençal front [*Prieur et al.*, 1993]; the adjacent ecosystems are comparable [*Claustre et al.*, 1994b; *Fiala et al.*, 1994; *Thibault et al.*, 1994]. Moreover, the chemical characteristic (mainly the nutrient concentrations) of the water masses at depth are similar. Thus it can be assumed that the effects of upward advection on these adjacent ecosystems would be similar.

Depth-integrated primary productions estimated by *Videau et al.* [1994] in the Mediterranean and modified Atlantic waters adjacent to the Almería-Oran front range between 0.5–0.7 g C m^{-2} d^{-1}, which are close to the computed primary production

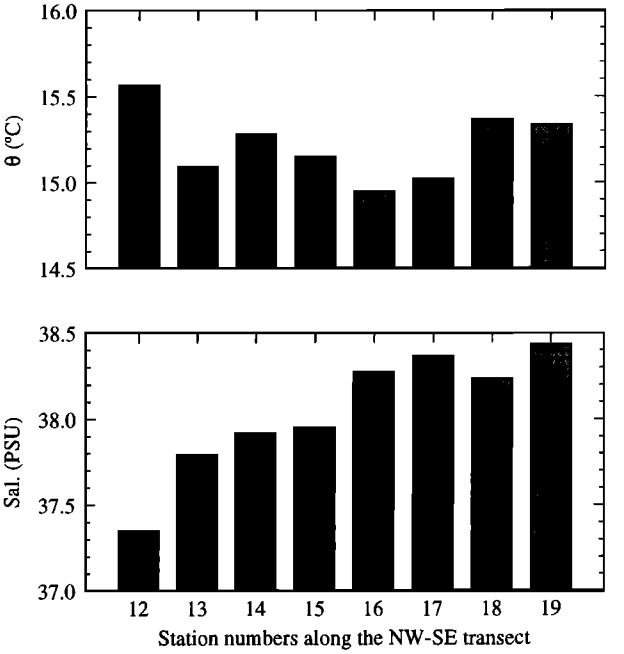

Figure 11. Potential temperature (θ) and salinity (Sal.) in subsurface (5 m depth) for THES transect PRO12–19.

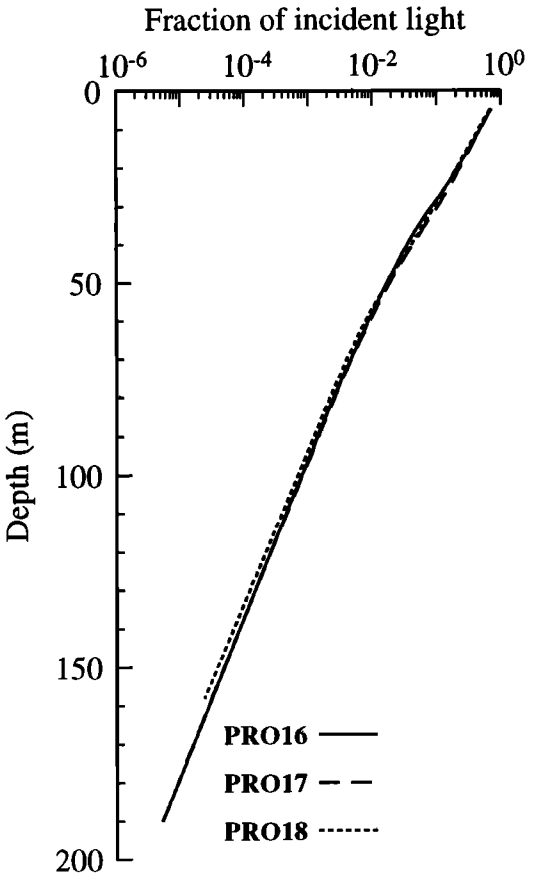

Figure 10. Light penetration at depth as a function of diffuse attenuation by sea water and chlorophyll *a* concentrations. We used averaged diffuse attenuation coefficients $\chi w = 0.05$ m^{-1} for sea water and $\chi c = 0.0518$ (Chl a)$^{-0.572}$ m^{-1} for chlorophyll *a* from *Morel* [1988].

for $W = 0$ (Figure 6). Inside the frontal zone, daily integrated productions are significantly higher and reach a maximum value of 2 g C m^{-2} d^{-1} at site 6 in the left limit of the jet (heavy side of the front). Note that the distance between the sites of higher and lower primary production is less than the typical space scale of the frontal zone, i.e., the barocline deformation radius, which is 15–20 km for the Almería-Oran front (L. Prieur, unpublished data, 1990). Several features indicating upward motion were observed at site 6, particularly a shallowing of the nitracline, and significant increases were observed in the deep Chl *a* maximum and depth-integrated nitrate assimilation [*L'Helguen et al.*, 1992; *Prieur et al.*, 1993; *Videau et al.*, 1994], which did not alter the LTR characteristics. In comparison with the simulations, upward advections of 1–2 m d^{-1} would be sufficient to explain the three-fold increase in depth-integrated primary production at site 6.

The deep maxima for total primary production of 100–150 mg C m^{-3} d^{-1} computed for such upward advections (Figure 5a) are greater than maximum primary production rates estimated by *Videau et al.* [1994] in the Almería-Oran front (60 mg C m^{-3} d^{-1} at site 6) or values reported by *Hecq et al.* [1986] in the Liguro-Provençal front off the Corsica coast (up to 70 mg C m^{-3} d^{-1}). This discrepancy between the computed and observed primary production rates may arise from several reasons. The first is inherent to the simplification of the model which cannot take into account the full complexity of a natural situation. Indeed, the model mainly considers the new production dominated phytoplankton population, mainly diatoms, which is generally found at depth or during the spring bloom. The phytoplankton population involved in regenerated production, which dominates in near surface waters and during the oligotrophic phase of the seasonal cycle, should have different physiological characteristics so that its response to an increased upward nitrate flux would be different. In that sense, the regenerated production may be slightly underestimated by the model. Certainly, a more complex model including two

different phytoplankton populations would give a better simulated f ratio. Particularly, changes in the specific composition of the phytoplankton population, i.e., change in the relative abundance of diatoms versus flagellates, in response to the increased upward flux of nitrate would have some effects on the productivity by affecting the balance between new and regenerated production. Diatoms are mainly responsible of the large Chl *a* variations observed in the two geostrophic fronts described in our paper, and the chemical signs we describe are related to new production involved variables (Chl *a*, NO_3, and O_2). Note also that the two communities (new versus regenerated production communities) are encountered in geostrophic fronts while, generally, only the diatoms population is involved in the highest productivity of the area [e.g., *Claustre et al.*, 1994b]. Likewise, a more complex biological model should permit to identify the processes that lead to the high observed nitrite concentration, but we believe those unidentified processes would not have a more pronounced effect on new production than has the upward advection of nitrate. Then, we think a more complex model would change results on f ratio, by changing the regenerated production amount, but not the new production one nor the distribution of associated chemical tracers (NO_3 and O_2) or the increase of Chl *a*.

Second, estimations of primary production by in situ deck incubations are conducted from bottle-cast samples and such discrete sampling may easily miss maxima of primary production and biomass as sharp as those computed by the model. Chl *a* concentrations in the incubation experiments of *Videau et al.* [1994] never exceed 1 mg m^{-3} while Chl *a* concentrations estimated from fluorescence-cast vertical profiles on the same sites, as during all the cruise, showed DCM of ~2–3 mg m^{-3} in the frontal zone [*Prieur and Sournia*, 1994; *Claustre et al.*, 1994a, b]. Moreover, in situ deck incubations isolate a fraction of the phytoplankton population in a confined volume, while in natural conditions when upward motions occur, this phytoplankton biomass will receive a continuous upward flux of nutrients. Note that the maximum primary production rate in the data from *Videau et al.* [1994] and *Hecq et al.* [1986] was found at depth and close to the deep Chl *a* maximum and the nitracline (see site 6 in the data from *Videau et al.* [1994] in contrast to sites 2, 4, and 5). Except for their lower intensity, these deep maxima for primary production are therefore in qualitative agreement with the simulations. Assuming a C/Chl *a* ratio of 40, the assimilation index for the simulated deep production maximum ranges between 30 and 70 mg C (mg Chl *a*)$^{-1}$ d^{-1} and are close to the values reported by *Videau et al.* [1994] and *Hecq et al.* [1986]. Likewise, changes in the relationship between the depth-integrated phytoplankton biomass and primary production were also observed by *Videau et al.* [1994] in the Almería-Oran front, which is consistent with the simulations. The daily-integrated assimilation number at site 6 of 56 mg C (mg Chl *a*)$^{-1}$ d^{-1} contrasts with the constant and lower values at the other sites (30–35 mg C (mg Chl *a*)$^{-1}$ d^{-1}). *Claustre et al.* [1994a, b] discussed the relationships between measured primary production and phytoplankton biomass from the same data and also noted the peculiarity of site 6. Again, a C/Chl *a* ratio of 40 will give a good agreement between the modeled and observed productivity. It can be concluded that the model gives realistic values for depth-integrated production and phytoplankton productivity by comparisons with similar conditions in the Almería-Oran and Liguro-Provençal front.

5. Discussion

Ecological interpretations of the simulations presented here are first subject to the hypothesis of stationary physical forcings, i.e., light, vertical turbulent mixing (through vertical stratification) and upward advection, during the time needed for the ecosystem to achieve a steady state. Given the rapid reaction of the simulated ecosystem under conditions of moderate upward advection (<30 days, see Figure 3), the seasonal variations of the light field can be excluded. Moreover, in such simulations, the timescale needed to achieve a steady state is probably overestimated, owing to the crude biological model [*Zakardjian and Prieur*, 1994]. While diurnal variations of light modify the photosynthetic capability of the phytoplankton cells, we stated it would not affect population dynamics. It is likely that diurnal variations of light affect the physiology of the cells at short timescales (less than a day), while the productivity of the population depends on processes whose timescales are greater than the doubling time of the phytoplankton cells (one day or more). In our simulations, production per unit of biomass, as the unit of the population growth, and photosynthesis, as the basis for cell growth, are linked through the timescale $t_c(z)$. Previous modeling studies have shown that the diurnal light cycle has little effect on simulations over periods of some tens of days [*Taylor et al.*, 1986; *Franks et al.*, 1986a; *Pribble et al.*, 1994]. This assumption is also valid for short-time variations of light due to the upward motions of the cells. Finally, the model supposes a uniform physiological adaptation of the phytoplankton cells during the simulations and focuses on processes affecting population dynamics and productions.

Second, it is unlikely that the stratification of the water column will remain constant under conditions of upward advection, which is supposed to shift the isopycnals toward the surface. Vertical motions in front, and more generally secondary circulations, are related to frontogenesis [*Mooers*, 1977; *Hoskins*, 1982], because of large-scale geostrophic forcings [e.g., *Woods*, 1988; *Bleck et al.*, 1988; *Pollard and Regier*, 1992] or wave-like instabilities of the geostrophic jet [e.g., *Onken*, 1992; *Wang*, 1993; *Barth*, 1994]. All these processes imply rapid time evolution of the density, velocity, and vorticity of the front. Curiously, the frontal structure observed during the Prolig 2 cruise was quite stable on a 10 day timescale, despite biological and chemical evidence for upward motions at station PRO16 and PRO17 (see section 4.1), as for several transects during the same cruise [*Zakardjian*, 1994]. The same paradox occurred during the Almofront 1 (1991) cruise. Biological evidence for vertical advective-like motions are described in several Almofront 1 related studies [*Prieur et al.*, 1993; *Claustre et al.*, 1994a, b; *Videau et al.*, 1994], while the thermohaline and dynamic characteristics of the frontal structures were stable along the jet and during this 6 week cruise [*Prieur and Sournia*, 1994; *Zakardjian*, 1994]. *Mooers* [1977] and *Fédorov* [1986] suggested that dissipation processes can lead to stationary density and velocity fields in fronts. The dissipation processes are not fully considered in models of oceanic frontogenesis while *Williams* [1974] described a model of a steady state atmospheric front in which turbulent mixing balances frontogenesis. Identifying the physical processes that would have advective-like signatures without altering the density field is not within the scope of this study, which only defines biological and chemical criteria that reveal such upward motion on the heavy side of both the Liguro-Provençal and Almería-Oran fronts. Nev-

ertheless, a recent study by *Pelegrí and Csanady* [1994] describes and analyzes the possible existence of advective-like motions across isopycnal surfaces on the heavy side of the Gulf Stream. *Lohrenz et al.* [1993] found consistently higher phytoplankton biomass and production on the slope water side (heavy side) of the Gulf Stream, both in the case of a meandering flow or a more linear stream. Such observations may support the results obtained here and raises the possibility of small-scale instabilities (see the density inversions at station PRO15 in Figure 7b and at station PRO16 in Figure 8), which would have advective-like signatures on biogeochemical tracers or would induce very localized upward velocities.

More critical is the fact that oceanic flows and particularly the secondary circulation of geostrophic fronts are fundamentally three-dimensional. Thus the upwelled advective flow can not remain constant over the whole water column and simply escapes in a 10 m thick mixed layer as in our simulations. In natural situations, lateral advective flows can export the phytoplankton biomass and nutrients out of the local water column from a large part of the water column. *Pribble et al.* [1994] and *Moisan and Hofmann* [1996] also used quasi-vertical, biophysical models to study the effect of vertical advection with vertical variations of W that are compensated by divergence or convergence terms. While more realistic, such divergence terms require assumptions about horizontal gradients of phytoplankton and nutrients concentrations [e.g., *Pribble et al.*, 1996]. Given the short spatial scale of the upward motion zones in the Liguro-Provençal and Almería-Oran fronts (less than the barocline deformation radius, see section 4.1 and 4.2) and the strong, cross-front, spatial heterogeneity observed during both the Prolig 2 and the Almofront 1 cruises [e.g., *Prieur and Sournia*, 1994; *Claustre et al.*, 1994b; *Zakardjian*, 1994], defining horizontal gradients would be difficult and, overall, subject to serious restrictions. For the present simulations, the most important factor affecting the dynamics of the phytoplankton-nutrient system is the upward flux of nitrate. Only the upward velocity in the euphotic layer is important for the shallowing of the phytoplankton-nutrient system of new production. That is to say that higher upward velocity at depth will be compensated by horizontal flow before it reaches the euphotic depth and may not induce higher upward nutrients fluxes in the biologically active upper layer. In that sense, the upward velocities deduced from the response of the simulated phytoplankton-nutrients system are lower bounds of the true dynamically induced upward velocities, which act on the entire water column.

The results of the simulations showed that low upward advections ($W < 4$ m d^{-1}) carried the phytoplankton-nutrients system of new production toward the surface without altering its main characteristics, i.e., the DBM coupled with the nitracline, but with an increase in phytoplankton biomass. Such features agree with previous modeling studies by *Wroblewski* [1977], *Franks et al.* [1986a], *Pribble et al.* [1994], or *Moisan and Hofmann* [1996]. The results of our simulations highlighted several additional features, mainly the shallowing of the O_2 and nitrite maxima and the sharpening of the nitracline, oxycline, and deep maxima for phytoplankton biomass, oxygen, and nitrite. These patterns are illustrated here by observations from a unique set of multiparametric and quasi-continuous data gathered in the Liguro-Provençal front. Higher upward advection can lead to a complete alteration of the LTR system for new production, as it confines the phytoplankton biomass to the upper mixed layer and leads to a breakdown of the DBM. The effects of high upward advection on oligotrophic-type ecosystems have been similarly described by *Wolf and Woods* [1988] using their nonsteady Lagrangian model, although the mathematical and physical approaches between our model and their model are different. Referring to the simulations (Figure 4), upward advections of 1–2 m d^{-1} would be sufficient to account for the shallowing of the nitracline and Chl a and O_2, maxima observed at stations PRO16 and PRO17. Such upward advections may also explain the two-fold increase in Chl a in going from station PRO18 to PRO16 as the deep Chl a maximum becomes shallower. By comparing the simulated primary production and measurements made in the Almería-Oran front, upward advections of 1–2 m d^{-1} would explain the three-fold increase in primary production observed on the heavy side of the front as described by *Videau et al.* [1994]. Since the model did not include sinking of phytoplankton cells, estimations of these upward advections may be slightly underestimated. Nevertheless, sinking rates for nonsenescent diatom cells are <2 m d^{-1} [*Smayda*, 1970] and would decrease in conditions of high-nutrient enrichment [e.g., *Bienfang*, 1981; *Bienfang et al.*, 1982]. *Pribble et al.* [1994] showed that the response of a phytoplankton-nutrient system to upward motion is insensitive to high sinking rates of phytoplankton aggregates.

In addition to the physical and biochemical signs discussed in the previous paragraph, an increase in the daily integrated assimilation ratio may be an indicator of enhanced new production resulting from upward motions in permanent geostrophic frontal zones. We have seen that this increase in the daily integrated assimilation ratio is due to the horizontal transport of a part of the newly produced phytoplankton biomass out of the local water column. This horizontal flux of phytoplankton biomass is ~6% of the computed new production for $W = 1$ m d^{-1} and reaches 54% for $W = 5$ m d^{-1}. By contrast, the BEM tends to be limited by the local amount of phytoplankton biomass (see Figure 3). This means that it can be a shift from a biological loss term (BEM) to an hydrodynamic one (F_s) to balance the increased new production in a one-dimensional vertical approach. This shift finally depends on the ability of the local ecosystem to exploit the phytoplankton biomass. In that sense, the use of a time-constant zooplankton biomass may introduce a bias in this interpretation, but the food-level acclimation that is inherent to the *Franks et al.* [1986b] grazing formulation may partly compensate this problem in our model. Moreover, as the residence time of the phytoplankton in the water column will decrease for increasing W, the advection loss term would tend to be more predominant. This implies that a significant amount of the newly produced phytoplankton biomass will accumulate in nearby waters. Hence the hypothesis of some front-induced enhancement of primary production is not contradictory with the accumulation hypothesis for the high biomass observed in frontal zones as defined by *Franks* [1992], which may prevail in tidal stirring induced fronts. In contrast with situations of enhanced primary production, accumulation zones are characterized by a decrease in the daily integrated assimilation number [e.g., *Pingree et al.*, 1975; *Videau*, 1987]. Indeed, the interpretation of the higher biomass observed in frontal zones ultimately depends on the spatial scale being investigated. The higher mean levels of phytoplankton biomass observed in the Liguro-Provençal and Almería-Oran frontal zones indicate a front-induced enhancement of primary production. In addition, the strong spatial heterogeneity of the integrated phytoplankton biomass inside the frontal zones

[e.g., *Prieur et al.*, 1993; *Claustre et al.*, 1994b] may result from spatially alternating upward and downward motion zones in which the two hypotheses of enhanced new production or biomass accumulation prevail, respectively. A main consequence is that the zones of higher new production and higher phytoplankton biomass may be spatially uncoupled at small scales in such frontal zones. This hypothesis also limits the applicability of quasi-vertical models for studying the effect of downward motions in frontal zones, as the biological and chemical characteristics of the downwelled waters result from an adjacent phytoplankton-nutrient system which has its own dynamics. By contrast, the response of the phytoplankton-nutrient system to an upward motion depends mainly on the nutrient concentrations at depth which are generally well-known and invariant with time.

6. Concluding Remarks

The simple model described here uses only the vertical stratification and the ecological response of a simulated, phytoplankton-nutrient system of primary production in order to evaluate and localize low upward motions by comparisons with observations. We used this diagnostic tool to evaluate the upward advections that are needed to explain the high biomass and primary production observed in both the Liguro-Provençal and the Almería-Oran fronts [*Hecq et al.*, 1986; *Sournia et al.*, 1990; *Prieur et al.*, 1993; *Videau et al.*, 1994; *Claustre et al.*, 1994a, b], as in other geostrophic fronts of the Western Mediterranean [e.g., *Johnson et al.*, 1989; *Raimbault et al.*, 1993]. As can be seen from our results, the upward motions in such frontal zones would lead to small scale spatial variabilities in the depth of the nitracline, the oxycline, the deep maxima of Chl *a*, O_2 and NO_2, and phytoplankton population productivity. Such small-scale variabilities were observed in both the Liguro-Provençal (examples presented in this study) and the Almería-Oran fronts, when an adequate sample strategy was employed [*Sournia et al.*, 1990; *Prieur et al.*, 1993; *Videau et al.*, 1994]. Low upward advections (1–2 m d^{-1}) in the euphotic layer would be sufficient to account for both these spatial variations and the observed increase in primary production in the Almería-Oran front, suggesting a great sensitivity for oligotrophic-type or LTR-type systems to upward motions. Such low upward motions can also be associated with wind induced Ekman pumping at mesoscale (atmospheric perturbations scale) in nonfrontal zones, as described by V. Andersen and L. Prieur (High frequency time series observations in the open northwestern Mediterranean Sea and effects of winds events (Dynaproc Study, May 1995), submitted to *Deep Sea Research*, 1997). This study also underlines the importance of advective flows that can spatially uncouple zones of high phytoplankton biomass and new production at small scales. Such an uncoupling may call into question again the notion of vertical station for frontal studies and strengthens the necessity for frontal-adapted, fine-scale sampling.

Appendix

System of differential equations and formulation of biological processes used for the spatial and temporal evolution of the state variables are shown

$$\frac{\partial B}{\partial t} + \frac{\partial W\,B}{\partial z} = \frac{\partial}{\partial z}\left[K\frac{\partial B}{\partial z}\right] + \mu B - \mathrm{Graz}(B) \quad \text{(A1)}$$

$$\frac{\partial \mathrm{NO_3}}{\partial t} + \frac{\partial W\,\mathrm{NO_3}}{\partial z} = \frac{\partial}{\partial z}\left[K\frac{\partial \mathrm{NO_3}}{\partial z}\right] - S_{\mathrm{NO3}}\mu B + R_2(\mathrm{NO_2}) \quad \text{(A2)}$$

$$\frac{\partial \mathrm{NO_2}}{\partial t} + \frac{\partial W\,\mathrm{NO_2}}{\partial z} = \frac{\partial}{\partial z}\left[K\frac{\partial \mathrm{NO_2}}{\partial z}\right] - S_{\mathrm{NO2}}\mu B + R_1(\mathrm{NH_4}) - R_2(\mathrm{NO_2}) \quad \text{(A3)}$$

$$\frac{\partial \mathrm{NH_4}}{\partial t} + \frac{\partial W\,\mathrm{NH_4}}{\partial z} = \frac{\partial}{\partial z}\left[K\frac{\partial \mathrm{NH_4}}{\partial z}\right] - S_{\mathrm{NH4}}\mu B + 0.6\mathrm{Graz}(B) - R_1(\mathrm{NH_4}) \quad \text{(A4)}$$

$$\frac{\partial \mathrm{O_2}}{\partial t} + \frac{\partial W\,\mathrm{O_2}}{\partial z} = \frac{\partial}{\partial z}\left[K\frac{\partial \mathrm{O_2}}{\partial z}\right] + [pq_1(1 - S_{\mathrm{NH4}}) + pq_2 S_{\mathrm{NH4}}]\mu B - \phi 0.6\mathrm{Graz}(B) - \alpha_1 R_1(\mathrm{NH_4}) - \alpha_2 R_2(\mathrm{NO_2}) \quad \text{(A5)}$$

$$S_{\mathrm{NO3}} + S_{\mathrm{NH4}} + S_{\mathrm{NO2}} = 1 \quad \text{(A6)}$$

$$\mathrm{BEM}(t) = L\int_0^{200} 0.4\mathrm{Graz}(B)\,\delta z \quad \text{(A7)}$$

$$\mathrm{Graz}(B) = \bar{Z}r_{\max}(\beta B)[1 - \exp(-\beta(B - S_b))]H(B, S_b) \quad \text{(A8)}$$

$$R_1[\mathrm{NH_4}] = R_{1\max}\frac{\mathrm{NH_4}}{\mathrm{NH_4} + K_R} \quad \text{(A9)}$$

$$R_2[\mathrm{NO_2}] = R_{2\max}\frac{\mathrm{NO_2}}{\mathrm{NO_2} + K_R} \quad \text{(A10)}$$

$$F(\mathrm{O_2}) = PV[O_2^{ML} - O_{2sat}] \quad \text{(A11)}$$

Acknowledgments. Financial support was received from INSU (Frontal/JGOFS-France), CNRS (URA 353), and DRET (contract 900 196). We wish to thank C. Copin-Montégut, P. Raimbault, P. LeCorre, and coworkers for help in processing and interpretation of THES data. Thanks to H. Claustre, P. Chang, and P. Lee for their valuable comments and reviews on the manuscript. We are grateful to S. E. Lohrenz for his very encouraging comments on the first version of this work.

References

Alcaraz, J. M., Summer zooplankton metabolism and its relation to primary productivity in the Western Mediterranean, in *Océanographie Pélagique Méditerranéenne*, edited by P. Nival and H. J. Minas, *Oceanol. Acta*, *9*, 185–191, 1988.

Andersen, V., and P. Nival, Modèle d'ecosystème pélagique des eaux côtières en Mer Ligure, in *Océanographie Pélagique Méditerranéennne*, edited by P. Nival and H. J. Minas, *Oceanol. Acta*, *9*, 211–217, 1988a.

Andersen, V., and P. Nival, A pelagic ecosystem model simulating production and sedimentation of biogenic particles: Role of salps and copepods, *Mar. Ecol. Prog. Ser.*, *44*, 37–50, 1988b.

Barth, J. A., Short-wavelength instabilities on coastal jets and fronts, *J. Geophys. Res.*, *99*, 16,095–16,115, 1994.

Berggreen, U., B. Hansen, and T. Kiørboe, Food size spectra, ingestion and growth of the copepod *Acartia tonsa* during development: Implications for determination of copepod production, *Mar. Biol.*, *99*, 341–352, 1988.

Béthoux, J. P., and L. Prieur, Hydrologie et circulation en Méditerranée nord-occidentale, *Pet. Tech.*, *299*, 25–34, 1983.

Bienfang, P. K., Sinking rates of heterogeneous, temperate phytoplankton populations, *J. Plankton Res.*, *3*, 235–253, 1981.

Bienfang, P. K., P. J. Harrison, and L. M. Quarmby, Sinking rate response to depletion of nitrate, phosphate and silicate in four marine diatoms, *Mar. Biol.*, *67*, 295–302, 1982.

Bleck, R., R. Onken, and D. Woods, A two-dimensional model of mesoscale frontogenesis in the ocean, *Q. J. R. Meteorol. Soc.*, *114*, 347–371, 1988.

Boucher, J., F. Ibanez, and L. Prieur, Daily and seasonal variations in the spatial distribution of zooplankton populations in relation to the physical structure in the Ligurian front, *J. Mar. Res.*, *45*, 133–173, 1987.

Cheney, R. E., and R. A. Doblar, Structure and variability of the Alboran Sea frontal system, *J. Geophys. Res.*, *87*, 585–594, 1982.

Claustre, H., and J. Gostan, Adaptation of biochemical composition and cell size to irradiance in two microalgae: Possible ecological implications, *Mar. Ecol. Prog. Ser.*, *40*, 167–174, 1987.

Claustre, H., P. Kerhervé, J. C. Marty, and L. Prieur, Phytoplankton photoadaptation related to some frontal physical processes, *J. Mar. Syst.*, *5*, 251–265, 1994a.

Claustre, H., P. Kerhervé, J. C. Marty, L. Prieur, C. Videau, and J. H. Hecq, Phytoplankton dynamics associated with a geostrophic front: Ecological and biogeochemical implications, *J. Mar. Res.*, *52*, 711–742, 1994b.

Collos, Y., Transient situations in nitrate assimilation by marine diatoms, 2, Changes in nitrate and nitrite following a nitrate perturbation, *Limnol. Oceanogr.*, *27*, 528–535, 1982.

Collos, Y., and G. Slawyk, Ammonium and nitrate in the tropical and equatorial Atlantic: Relations with the primary nitrite maximum, *Mar. Bio. Lett.*, *4*, 295–308, 1983.

Cullen, J. J., The deep chlorophyll maximum: Comparing vertical profiles of chlorophyll a, *Can. J. Fish. Aquat. Sci.*, *39*, 791–803, 1981.

Cummins, P. F., G. Holloway, and A. E. Gargett, Sensitivity of the GFDL ocean general circulation model to a parameterization of vertical diffusion, *J. Phys. Oceanogr.*, *20*, 817–830, 1990.

Denman, K. L., and A. E. Gargett, Time and space scales of vertical mixing and advection of phytoplankton in the upper ocean, *Limnol. Oceanogr.*, *28*, 801–815, 1983.

Dewey, R. K., J. N. Moum, V. A. Paulson, D. R. Caldwel, and S. D. Piera, Structures and dynamics of a coastal filament, *J. Geophys. Res.*, *96*, 14,885–14,907, 1991.

Dortch, Q., The interaction between ammonium and nitrate uptake in phytoplankton, *Mar. Ecol. Prog. Ser.*, *61*, 183–201, 1990.

Eppley, R. W., and B. J. Peterson, Particulate organic matter flux and planktonic new production in the deep ocean, *Nature*, *282*, 677–680, 1979.

Eppley, R. W., J. N. Rogers, and J. J. McCarthy, Half-saturation constants for uptake of nitrate and ammonium by marine phytoplankton, *Limnol. Oceanogr.*, *14*, 912–920, 1969.

Falkowski, P. G., Z. Dubinsky, and K. Wyman, Growth-irradiance relationships in phytoplankton, *Limnol. Oceanogr.*, *30*, 311–321, 1985.

Fasham, M. J. R., and P. R. Pugh, Observations of the horizontal coherence of chlorophyll-a and temperature, *Deep Sea Res. Oceanogr. Abstr.*, *23*, 527–538, 1976.

Fédorov, K. N., *The Physical Nature and Structure of Oceanic Fronts*, vol 19, *Lecture Notes on Coastal and Estuarine Studies*, 333 pp., Springer-Verlag, New York, 1986.

Fiala, M., A. Sournia, H. Claustre, J.-C. Marty, L. Prieur, and G. Vétion, Gradients of phytoplankton abundance, composition and photosynthetic pigments across the Almeria-Oran front (SW Mediterranean Sea), *J. Mar. Syst.*, *5*, 223–233, 1994.

Franks, P. J. S., Sink or swim: Accumulation of biomass at fronts, *Mar. Ecol. Prog. Ser.*, *82*, 1–12, 1992.

Franks, P. J. S., J. S. Wroblewski, and G. R. Flierl, Prediction of phytoplankton growth in response to the frictional decay of a warm-core ring, *J. Geophys. Res.*, *91*, 7603–7610, 1986a.

Franks, P. J. S., J. S. Wroblewski, and G. R. Flierl, Behavior of a simple plankton model with food-level acclimation by herbivores, *Mar. Biol.*, *91*, 121–129, 1986b.

Frost, B. W., Grazing, in *The Physiological Ecology of Phytoplankton*, edited by I. Moriss, pp. 465–491, Univ. of Calif. Press, Berkeley, 1980.

Gargett, A. E., and G. Holloway, Dissipation and diffusion by internal wave breaking, *J. Mar. Res.*, *24*, 15–27, 1984.

Gaspar, P., Y. Gregoris, R. Stull, and C. Boissier, Long term simulation of upper ocean mixing using models of different types, in *Small Scale Turbulence and Mixing in the Upper Ocean*, edited by J. C. J. Nihoul and B. Jamart, *Elsevier Oceanogr. Ser., Amsterdam*, *46*, 169–184, 1988.

Hecq, J. H., J. M. Bouquegneau, S. Djenidi, M. Frankignoulle, A. Goffart, and M. Licot, Some aspects of the liguro-provencal frontal ecohydrodynamics, in *Marine Interfaces Hydrodynamics*, edited by J. C. J. Nihoul, *Elsevier Oceanogr. Ser., Amsterdam*, *42*, 257–271, 1986.

Hood, R. R., and D. B. Olson, A numerical investigation of diffusion, sinking and remineralization in an oligotrophic system, *Eos Trans. AGU*, *75*(3), Ocean Sci. Meet. Suppl., 95, 1994.

Hoskins, B. J., The mathematical theory of frontogenesis, *Ann. Rev. Fluid Mech.*, *14*, 131–151, 1982.

Johnson, K. S., S. W. Willason, D. A. Wiesenburg, S. E. Lohrenz, and R. A. Arnone, Hydrogen peroxide in the western Mediterranean Sea: A tracer for vertical advection, *Deep Sea Res., Part A*, *36*, 241–254, 1989.

Jones, B. H., and D. Halpern, Biological and physical aspects of a coastal upwelling event observed during March–April 1974 off northwest Africa, *Deep Sea Res., Part A*, *28*, 71–82, 1981.

Kaplan, W. A., Nitrification, in *Nitrogen in the Marine Environment*, edited by E. J. Carpenter and D. G. Capone, pp. 347–384, Academic, San Diego, Calif., 1983.

Kiefer, D. A., and B. G. Mitchell, A simple steady state description of phytoplankton growth based on absorption cross section and quantum efficiency, *Limnol. Oceanogr.*, *28*, 770–776, 1983.

Kiørboe, T., Phytoplankton growth rate and nitrogen content: Implications for feeding and fecundity in an herbivorous copepod, *Mar. Ecol. Prog. Ser.*, *55*, 229–234, 1989.

Lande, R., and A. M. Wood, Suspension times of particles in the upper ocean, *Deep Sea Res., Part A*, *34*, 61–72, 1987.

Laws, E. A., and T. T. Bannister, Nutrient- and light-limited growth of *Thalassiosira fluviatilis* in continuous culture, with implications for phytoplankton growth in the ocean, *Limnol. Oceanogr.*, *25*, 457–473, 1980.

L'Helguen, S., C. Madec, and P. LeCorre, Flux d'azote dans la zone du front Almeria-Oran: Absorption et régénération (mesures par l'azote 15), in *Processes and Budgets in Geostrophic Fronts, JGOFS-France, Rapp.*, *13*, 76–80, 1992.

Lohrenz, S. E., D. A. Wiesenburg, I. P. DePalma, K. S. Johnson, and D. E. Gustafson, Interrelationships among primary production, chlorophyll, and environmental conditions in frontal regions of the Western Mediterranean Sea, *Deep Sea Res., Part A*, *35*, 793–810, 1988.

Lohrenz, S. E., J. J. Cullen, D. A. Phinney, D. B. Olson, and C. S. Yentsch, Distributions of pigments and primary production in a Gulf Stream meander, *J. Geophys. Res.*, *98*, 14,545–14,560, 1993.

Longhurst, A. R., and W. G. Harrison, The biological pump: Profiles of plankton production and consumption in the upper ocean, *Prog. Oceanog.*, *22*, 47–123, 1989.

McCarthy, J. J., Nitrogen, in *The physiological ecology of phytoplankton*, edited by I. Morris, pp. 191–234, Univ. of Calif. Press, Berkeley, 1980.

Moisan, J. R., and E. E. Hofmann, Modeling nutrient and plankton processes in the California coastal transition zone, 1, A time- and depth-dependent model, *J. Geophys. Res.*, *101*, 22,647–22,676, 1996.

Mooers, C. N. K., Frontal dynamics and frontogenesis, in *Oceanic Fronts in Coastal Processes*, edited by M. J. Bowman and W. E. Esaias, pp. 16–22, Springer-Verlag, New York, 1977.

Morel, A., Optical modeling of the upper ocean in relation to its biogenous matter content (case I waters), *J. Geophys. Res.*, *93*, 10,749–10,768, 1988.

Moum, J. N., and T. R. Osborn, Mixing in the main thermocline, *J. Phys. Oceanogr.*, *16*, 1250–1259, 1986.

Olson, R. J., ^{15}N tracer studies of the primary nitrite maximum, *J. Mar. Res.*, *39*, 203–226, 1981.

O'Neill, R. V., D. L. DeAngelis, J. J. Pastor, B. J. Jackson, and W. M. Post, Multiple nutrient limitations in ecological models, *Ecol. Modell.*, *46*, 147–163, 1989.

Onken, R., Mesoscale upwelling and density finestructure in the seasonal thermocline: A dynamical model, *J. Phys. Oceanogr.*, *22*, 1257–1273, 1992.

Osborn, T. R., Estimates of the local rate of vertical diffusion from dissipation measurements, *J. Phys. Oceanogr.*, *10*, 83–89, 1980.

Pelegrí, J. L., and G. T. Csanady, Diapycnal mixing in western boundary currents, *J. Geophys. Res.*, *99*, 18,275–18,304, 1994.

Pingree, R. D., and G. T. Mardell, Solitary internal waves in the Celtic Sea, *Prog. Oceanogr.*, *14*, 431–444, 1985.

Pingree, R. D., P. R. Pugh, P. M. Holligan, and G. R. Forster, Summer phytoplankton blooms and red tides along tidal fronts in the approaches to the English Channel, *Nature*, *258*, 672–677, 1975.

Pollard, R. T., and L. A. Regier, Vorticity and vertical circulation at an ocean front, *J. Phys. Oceanogr.*, *22*, 609–625, 1992.

Pomeroy, L. R., and W. J. Wiebe, Energetics of microbial food webs, *Hydrobiologia*, *159*, 7–18, 1988.

Pribble, J. R., J. J. Walsh, and D. A. Dieterle, A numerical analysis of shipboard and coastal zone color scanner time series of new production within Gulf Stream cyclonic eddies in the South Atlantic Bight, *J. Geophys. Res.*, *99*, 7513–7538, 1994.

Prieur, L., Systèmes frontaux en Mer Ligure à partir des mesures multiparamétriques en continu, Le Courrier de Mediprod, n°2, Lab. Arago, Banyuls, France, 1985.

Prieur, L., and L. Legendre, Oceanographic criteria for new phytoplankton production, *Toward a Theory on Biological-Physical Interactions in the World Ocean*, edited by B. J. Rotschild, pp. 71–112, Kluwer Acad., Norwell, Mass., 1988.

Prieur, L., and S. Sathyendranath, An optical classification of coastal and oceanic waters based on the specific spectral absorption curves of phytoplankton pigments, dissolved organic matter, and other particulate materials, *Limnol. Oceanogr.*, *26*, 671–689, 1981.

Prieur, L., and A. Sournia, Almofront-1 (April–May 1991): An interdisciplinary study of the Almeria-Oran front, SW Mediterranean Sea, *J. Mar. Syst.*, *5*, 187–203, 1994.

Prieur, L., C. Copin-Montégut, and H. Claustre, Biophysical aspects of "ALMOFRONT-I," An intensive study of a geostrophic frontal jet, *Annl. Inst. Oceanogr.*, *69*, 71–86, 1993.

Raimbault, P., B. Coste, M. Boulhadid, and B. Boudjellal, Origin of high phytoplankton concentration in deep chlorophyll maximum (DCM) in a frontal region of the Southwestern Mediterranean Sea (Algerian Current), *Deep Sea Res., Part A*, *40*, 791–804, 1993.

Redfield, A. C., B. H. Ketchum, and F. A. Richards, The influence of organisms on the composition of sea water, in *The Sea, Ideas and Observations on Progress in the Study of the Seas*, edited by M. N. Hill, pp. 26–27, Wiley-Interscience, New York, 1963.

Richardson, K., J. Beardall, and J. A. Raven, Adaptation of unicellular algae to irradiance: An analysis of strategies, *New Phytol.*, *9*, 157–191, 1983.

Roach, P. J., *Computational Fluid Dynamics*, 446 pp., Hermosa, Albuquerque, N. M., 1972.

Sharples, J., and P. Tett, Modelling the effect of physical variability on the midwater chlorophyll maximum, *J. Mar. Res.*, *52*, 219–238, 1994.

Small, L. F., and D. W. Menzies, Patterns of primary production and biomass in a coastal upwelling region, *Deep Sea Res., Part A*, *28*, 123–150, 1981.

Small, L. F., S. W. Fowler, S. A. Moore, and J. LaRosa, Dissolved and fecal pellet carbon and nitrogen release by zooplankton in tropical waters, *Deep Sea Res., Part A*, *30*, 1199–1220, 1983.

Smayda, T. J., The suspension and sinking of phytoplankton in the sea, *Oceanogr. Mar. Biol.*, *8*, 353–414, 1970.

Sournia, A., J. M. Brylinski, S. Dallot, P. LeCorre, M. Leveau, L. Prieur, and C. Froget, Fronts hydrologiques au large des côtes françaises: Les sites ateliers du programme Frontal, *Oceanol. Acta*, *13*, 413–438, 1990.

Taylor, A. H., J. R. W. Harris, and J. Aiken, The interaction of physical and biological processes in a model of the vertical distribution of phytoplankton under stratification, in *Marine Interfaces Hydrodynamics*, edited by J. C. J. Nihoul, *Elsevier Oceanogr. Ser.*, Amsterdam, *42*, 313–330, 1986.

Thibault, D., R. Gaudy, and J. Le Fèvre, Zooplankton biomass, feeding and metabolism in a geostrophic frontal area (Almeria-Oran Front, western Mediterranean): Significance to pelagic food webs, *J. Mar. Syst.*, *5*, 297–311, 1994.

Tintoré, J., P. E. La Violette, I. Blade, and A. Cruzado, A study of an intense density front in the Eastern Alboran Sea: The Almeria-Oran front, *J. Phys. Oceanogr.*, *18*, 1384–1397, 1988.

Tintoré, J., D. Gomis, and S. Alonso, Mesoscale dynamics and vertical motion in the Alborán Sea, *J. Phys. Oceanogr.*, *21*, 811–823, 1991.

Varela, R. A., A. Cruzado, J. Tintoré, and E. Garcia Ladona, Modelling the deep-chlorophyll maximum: A coupled physical-biological approach, *J. Mar. Res.*, *50*, 441–436, 1992.

Varela, R. A., A. Cruzado, and J. Tintoré, A simulation analysis of various biological and physical factors influencing the deep-chlorophyll maximum structure in oligotrophic areas, *J. Mar. Syst.*, *5*, 143–157, 1994.

Videau, C., Primary production and physiological state of phytoplankton at the Ushant tidal front (west coast of Brittany, France), *Mar. Ecol. Progr. Ser.*, *35*, 141–151, 1987.

Videau, C., A. Sournia, L. Prieur, and M. Fiala, Phytoplankton and primary production characteristics at selected sites in the geostrophic Almeria-Oran front system (SW Mediterranean Sea), *J. Mar. Syst.*, *5*, 235–250, 1994.

Viudez, A., and J. Tintoré, Circulation in the Alboran Sea as determined by quasi-synoptic hydrographic observations, 1, Three dimensional structure of the two anticyclonic gyres, *J. Phys. Oceanogr.*, *26*, 684–705, 1996.

Wada, E., and A. Hattori, Nitrite metabolism in the euphotic layer of the central north Pacific Ocean, *Limnol. Oceanogr.*, *16*, 766–772, 1971.

Wang, D.-P., Model of frontogenesis: Subduction and upwelling, *J. Mar. Res.*, *51*, 497–513, 1993.

Ward, B. B., Nitrogen transformations in the Southern California Bight, *Deep Sea Res., Part A*, *34*, 785–805, 1987.

Williams, P. J. le B., Raine, R. C. T. and Bryan, J. R., Agreement between the ^{14}C and the oxygen methods of measuring phytoplankton production: Reassessment of the photosynthetic quotient, *Oceanol. Acta*, *2*, 411–416, 1979.

Williams, R. T., Numerical simulation of steady-state fronts, *J. Atmos. Sci.*, *31*, 1286–1296, 1974.

Wolf, K. U., and J. D. Woods, Lagrangian simulation of primary production in the physical environment: The deep chlorophyll maximum and nutricline, in *Toward a Theory on Biological-Physical Interactions in the World Ocean*, edited by B. J. Rothschild, pp. 51–70, Kluwer Acad., Norwell, Mass., 1988.

Woods, J., Scale upwelling and primary production, in *Toward a Theory on Biological-Physical Interactions in the World Ocean*, edited by B. J. Rothschild, pp. 7–38, Kluwer Acad., Norwell, Mass., 1988.

Wroblewski, J. S., A model of phytoplankton plume formation during variable Oregon upwelling, *J. Mar. Res.*, *35*, 357–394, 1977.

Zakardjian, B., Rôle du système advection/diffusion sur la production primaire en zone frontal, Ph.D. thesis, 183 pp., Univ. Paris VI, 1994.

Zakardjian, B., and L. Prieur, A numerical study of primary production related to vertical mixing with special reference to vertical motions of phytoplankton cells in nutrient and light fields, *J. Mar. Syst.*, *5*, 267–295, 1994.

L. Prieur, Laboratoire de Physique et Chimie Marines, Observatoire Océanologique, URA 2076, CNRS, Université Paris VI, BP 08, 06238, Villefranche-sur-Mer cédex, France.

B. Zakardjian, Institut National de la Recherche Scientifique-Océanologie, Université du Québec à Rimouski, 310 Allée des Ursulines, Rimouski, Québec, G5L 3A1, Canada. (e-mail: Bruno_Zakardjian@UQAR.UQuebec.ca)

(Received October 10, 1997; revised April 22, 1998; accepted May 7, 1998.)